HHS Public Access

Author manuscript

Dev Biol. Author manuscript; available in PMC 2018 December 01.

Published in final edited form as:

Dev Biol. 2017 December 01; 432(1): 178–191. doi:10.1016/j.ydbio.2017.09.038.

Motor axons are guided to exit points in the spinal cord by Slit and Netrin signals

Minkyung Kim[*], **Tatiana M Fontelonga**, **Clare H Lee**, **Sarah J Barnum**, and **Grant S Mastick**

Department of Biology, University of Nevada, Reno, NV 89557, USA

Abstract

In the spinal cord, motor axons project out the neural tube at specific exit points, then bundle together to project toward target muscles. The molecular signals that guide motor axons to and out of their exit points remain undefined. Since motor axons and their exit points are located near the floor plate, guidance signals produced by the floor plate and adjacent ventral tissues could influence motor axons as they project toward and out of exit points.

The secreted Slit proteins are major floor plate repellents, and motor neurons express two Slit receptors, Robo1 and Robo2. Using mutant mouse embryos at early stages of motor axon exit, we found that motor exit points shifted ventrally in Robo1/2 or Slit1/2 double mutants. Along with the ventral shift, mutant axons had abnormal trajectories both within the neural tube toward the exit point, and after exit into the periphery. In contrast, the absence of the major ventral attractant, Netrin-1, or its receptor, DCC caused motor exit points to shift dorsally. Netrin-1 attraction on spinal motor axons was demonstrated by *in vitro* explant assays, showing that Netrin-1 increased outgrowth and attracted cultured spinal motor axons.

The opposing effects of Slit/Robo and Netrin-1/DCC signals were tested genetically by combining Netrin-1 and Robo1/2 mutations. The location of exit points in the combined mutants was significantly recovered to their normal position compared to Netrin-1 or Robo1/2 mutants. Together, these results suggest that the proper position of motor exit points is determined by a "push-pull" mechanism, pulled ventrally by Netrin-1/DCC attraction and pushed dorsally by Slit/Robo repulsion.

Keywords

spinal cord; motor exit points; floor plate; Slit/Robo; Netrin-1/DCC

[*]Corresponding author: Department of Biology, University of Nevada, 1664 N. Virginia St., Reno, NV 89557. Tel.: 775-784-6356; Fax: 775-784-1302.minkim@unr.edu.

Introduction

In the spinal cord, motor axons project out the neural tube at specific exit points, then bundle together to navigate through the periphery to form the motor nerves. A few reports showed that vertebrate transcription factors are required for guiding ventral motor neuron (vMN) and dorsal motor neuron (dMN) axons to their exit points. For instance, Lhx3/Lhx4 are required for directing vMN axons to their exit point (Sharma et al., 1998) and Phox2b is necessary for dMN axons to exit the spinal cord (Hirsch et al., 2007). In addition, genetic inactivation of Cxcl12 (SDF-1)-Cxcr4 signaling leads to atypical vMN axon growth to dorsal exit points, suggesting that Cxcl12-Cxcr4 signals direct vMN axons to normal exit points (Lieberam et al., 2005). However, it remains unknown which extrinsic guidance cues set the precise position of motor axon exit in the neural tube.

Spinal motor neurons differentiate from progenitor cells located in the ventricular zone of the ventral spinal cord, then settle near the floor plate. The neurons then very quickly project axons to a narrow area on the pial surface, penetrating the basement membrane to exit, while bundling together to form their peripheral motor nerve. The precise location of motor exit points in each spinal cord segment is critical for forming cohesive motor nerves, but the mechanisms that define motor exit points remain poorly understood. Motor neurons and their initial axon projections are exposed to several guidance cues. The floor plate and nearby tissues produce several types of guidance cues with well-known roles in guiding developing axons (Colamarino and Tessier-Lavigne, 1995b; Stein and Tessier-Lavigne, 2001). Commissural and longitudinal axons navigate through the neural tube responding to these secreted signals (Farmer et al., 2008; Kim et al., 2014; Serafini et al., 1996; Shoja-Taheri et al., 2015; Ypsilanti et al., 2010). The secreted Slit proteins are major repellents produced by the ventral midline and are expressed along the anteroposterior axis (Brose et al., 1999; Rothberg et al., 1990), and the Slit receptors Robo1 and Robo2 are expressed by motor neurons (Brose et al., 1999; Hammond et al., 2005; Kim et al., 2015; Lee et al., 2015). The major ventral attractant, Netrin-1, and its receptor DCC, guide axons and several types of neuron migration (Culotti and Merz, 1998; Kawasaki et al., 2006; Serafini et al., 1996; Yee et al., 1999). While Netrin-1 was thought to be derived primarily from the floor plate, and secreted to form a long range ventral-high gradient, recent studies provided evidence that the ventricular zone of spinal cord progenitor cells presents the crucial Netrin-1 cues to promote ventral growth of commissural axons toward the floor plate (Dominici et al., 2017; Varadarajan et al., 2017).

Several lines of evidence suggest that motor axons are guided by cues within the ventral spinal cord (Bai et al., 2011; Cowan et al., 2000; Hammond et al., 2005; Varela-Echavarría et al., 1997). Indeed, *in vitro* experiments showed that cultured spinal motor axons can respond to Slit signals (Bai et al., 2011). Interestingly, however, they reported that explanted spinal cord motor axons were unresponsive to Netrin-1 because of an activity of the Presenilin (PS1) secretase complex that cleaves DCC receptors (Bai et al., 2011). A recent report showed that Nkx2.9 controls spinal accessory motor axon projections to their lateral exit from the spinal cord by regulating Slit/Robo2 signaling (Bravo-Ambrosio et al., 2012). Together, these findings imply that guidance cues within the ventral spinal cord have the potential to set the precise position of motor exit points.

We have therefore investigated whether Slit and Netrin-1 signals are involved in guiding ventral motor exits in the spinal cord, by analyzing mouse embryos with mutations in these cues or their receptors, and assaying direct *in vitro* effects on cultured spinal motor axons. Our results suggest that the proper position of motor axon exits is determined by a balance between a ventral pull by Netrin-1/DCC attraction and a dorsal push by Slit/Robo repulsion.

Materials and Methods

Mouse embryos

Mouse experiments were carried out in accordance with the National Institutes of Health Guide for the Care and Use of Laboratory Animals, by protocols approved by the University of Nevada, Reno Institutional Animal Care and Use Committee. Embryonic day 9.5 (E9.5), 9.75 (E9.75), 10 (E10), 10.5 (E10.5), and 12.5 (E12.5) embryos were obtained via uterine dissection. Wildtype CD-1 mice (6–8 weeks old) were purchased from Charles River Laboratories (Wilmington, MA USA). The Robo (Grieshammer et al., 2004; Long et al., 2004; López-Bendito et al., 2007), Slit (Plump et al., 2002), Netrin-1 (Serafini et al., 1996), and DCC (Fazeli et al., 1997) mutant strains were gifts of Marc Tessier-Lavigne, Genentech, and Frederic Charron, ICMR, Montreal CA. Robo and Slit PCR genotyping were performed as previously described (Grieshammer et al., 2004; Long et al., 2004; López-Bendito et al., 2007; Plump et al., 2002). Netrin-1 and DCC genotyping were performed as previously described (Fazeli et al., 1997; Serafini et al., 1996). The Islet-1^{MN}-GFP-F strain was a gift of Samuel Pfaff (Lewcock et al., 2007), Salk Institute, and was crossed into CD1, Robo1/2 and Netrin-1 mutant backgrounds.

Genotyping for Netrin/Robo combination mutants

To produce triple knockout embryos, we obtained Netrin-1;Robo1;Robo2 triple heterozygous mice. An interesting challenge was to genotype combined mutants, because in contrast to the PCR genotyping with the Robo alleles, the Netrin-1 mutant allele is a LacZ/βgal gene trap which has not been precisely mapped (Serafini et al., 1996). In addition, the Robo1 mutant allele has the same LacZ/βgal cassette insert as Netrin-1 (Long et al., 2004; Serafini et al., 1996), so that PCR genotyping was not able to distinguish the Netrin-1 mutant allele in combined mutant embryos. We used X-gal labeling for genotyping Netrin-1 (Charron et al., 2003). Though the Robo1 and 2 mutant alleles both also include LacZ/βgal inserts, we found that only the Netrin-1 lacZ allele produced X-gal labeling in the floor plate and was thus sufficient for Netrin-1 genotyping of combined mutants. *Netrin-1*$^{-/-}$ embryos were confirmed by reduction or loss of commissural axons in spinal cord sections using βIII-tubulin labeling. We also performed β-galactosidase and Netrin-1 immunostaining on spinal cord sections to verify their genotypes (Table 1).

As combined Netrin-1 and Robo mutations caused a lethal genetic interaction, we obtained only one Netrin-1/Robo1/2 triple homozygous mutant embryos even though they are predicted at 1/16 ratios, which we previously reported (Kim et al., 2014). The triple mutant had the Netrin-1^{-} and β-galactosidase^{+} floor plate (Fig. 9A′, B′). Also, commissural axons were almost gone in the spinal cord (Fig. 9C′). These phenotypes were not observed in

Netrin-1$^{+/-}$;*Robo1*$^{-/-}$;*2*$^{-/-}$ embryos, which had Netrin-1^{+} floor plate and normal pre-crossing commissural axons (Fig. 9A, C).

Immunohistochemistry

For cryostat section immunolabeling, embryos were embedded in 15% sucrose/7.5% gelatin solutions, frozen, and then sectioned at 16 μm for E9.5 through E10.5 spinal cords (40 μm for E12.5) using a cryostat (Leica). To melt gelatin off of tissue sections, slides were placed in warm (37–45°C) 0.1 M phosphate buffer for a couple of minutes. Sections were washed for 30 min to an hour in PBS containing 1% normal goat serum and 0.1% Triton X-100 (PBST). Primary antibodies [rabbit anti-βIII-tubulin (Covance, 1:1000), rabbit anti-β-galactosidase (Cappel, 1:1000), rabbit anti-GFP (Invitrogen, 1:500), rabbit anti-Robo1 and Robo2 (kind gift of Elke Stein, Yale, 1:10,000), mouse anti-Islet-1 (DSHB, 1:100), goat anti-DCC (Santa Cruz, 1:250), rabbit anti-Netrin (gift from Tim Kennedy, Montreal, 1:500 (Kennedy et al., 2006))] were applied in PBST, and then slides incubated in a humidified chamber for 4 hours to overnight. After washing several hours in PBST, secondary antibodies (Jackson Immuno Laboratories) were applied for 2 hours, followed by several washes.

In situ hybridization

In situ hybridization was carried out using standard procedures (Mastick et al., 1997). Probes for Slit1 and Slit2 were provided by Marc Tessier-Lavigne (Rockefeller University, New York, NY).

Explant assay

Isl1-GFP^{+} spinal nuclei of E11 *Islet-1*^{MN}*-GFP-F* at the brachial level of the spinal cord were dissected to exclude the floor plate under a fluorescence dissecting microscope (Leica M165 FC). Culture conditions for explants were as described previously (Charron et al., 2003). To assay axon outgrowth, explants were cultured with or without Netrin-1 (200 ng/ml) for 48 hours. To assay directional effects, localized Netrin-1 sources were provided as described in our previous paper (Kim et al., 2014). Explants are co-cultured with aggregates of COS-7 cells transfected with no plasmid (mock) or Netrin-1 expression plasmid (gift of Marc Tessier-Lavigne, Rockefeller) for 48 hours.

The length of axons and number of axons were measured using the ImageJ plugin Neuron J as described in our previous paper (Kim et al., 2014). For the directional analysis, quadrants were marked on images using Adobe Illustrator (San Jose, CA), then imported and quantitated in Image J (NIH, Bethesda, MD).

Quantification of motor exit point defects

The position of motor exit points was measured at the brachial level of the spinal cord to consistently compare an equivalent level of the spinal cord. The measurements were made on βIII-tubulin labeled sections. TIFF images were imported into Image J to measure the position of motor axon exits. The circumferential distance from the ventral midline to the most ventral bundle at exit points was quantified and averaged (d_{mv}). Also, the circumferential distance from the ventral midline to the average position of all of the exiting

motor axon bundles was quantified and averaged (d_{ma}). Three spinal cord sections from each embryo were used for the measurement. To normalize for embryo size, the distance was divided by the embryo height (d_h, distance between the dorsal–ventral midlines). The average normalized distance ($d_{nv} = d_{mv}/d_h$ or $d_{na} = d_{ma}/d_h$) for each embryo was then used to perform statistical analysis. We carried out a power analysis (PS version 3.1.2, 2014) using $\alpha = 0.05$ and a power value of 0.8 for the t-statistics and revealed that minimum number of sample size of 4 can be reached to measure the statistically significant difference.

To examine the distribution of internal motor axon trajectories, each angle of Isl1-GFP$^+$ individual axon was measured at the brachial level of the spinal cord of E10 *Robo1*$^{+/+}$; *2*$^{+/+}$*::Islet-1*^{MN}*-GFP-F, Robo1*$^{-/-}$;*2*$^{-/-}$*::Islet-1*^{MN}*-GFP-F, Netrin-1*$^{+/+}$*::Islet-1*^{MN}*-GFP-F,* and *Netrin-1*$^{-/-}$*::Islet-1*^{MN}*-GFP-F*. The measurements were presented in Rose histograms using Matlab Version 8.5.0.197613 (R2015a). Angles of each projection were clustered in 10° bins. The length of each segment represented the percentage of total angles per bin.

To determine fasciculation of exit points in the spinal cord, the thickness of exit points was measured at the location where motor axons exit the spinal cord using E10 and E12.5 *Robo1*$^{+/+}$;*2*$^{+/+}$*::Islet-1*^{MN}*-GFP-F, Robo1*$^{-/-}$;*2*$^{-/-}$*::Islet-1*^{MN}*-GFP-F, Netrin-1*$^{+/+}$*::Islet-1*^{MN}*-GFP-F,* and *Netrin-1*$^{-/-}$*::Islet-1*^{MN}*-GFP-F*.

All image analysis was conducted by an observer blind to the genotype. Data are expressed as means + S.E.M, and differences tested for significance using student *t*-tests to analyze two groups. Data sets were tested for significance using ANOVA with Tukey's *post hoc* tests to analyze multiple groups. Data are considered significantly different from the control values were when $P < 0.05$.

Results

Robo1 and Robo2 are expressed by spinal motor neurons

Since the secreted Slit proteins are major repellents produced by the floor plate, and the Robo1 and Robo2 receptors mediate Slit repulsion in the spinal cord (Stein and Tessier-Lavigne, 2001), we first wanted to verify if Robo receptors are expressed by spinal motor neurons during the earliest stages of motor axon outgrowth and establishment of the motor exit points. As the Robo1 mutant allele has a β-geo insertion and Robo2 has a LacZ-tau insertion (Long et al., 2004), we labeled with β-galactosidase antibody and Islet-1 on *Robo1*$^{+/-}$ and *Robo2*$^{+/-}$ spinal cord sections at the brachial region (n=4 embryos for each genotype). Both *Robo1*$^{+/-}$ and *Robo2*$^{+/-}$ spinal motor neuron cell bodies and their axons were β-galactosidase$^+$, suggesting that Robo1 and Robo2 are expressed by Islet-1$^+$ spinal motor neuron cell bodies and axons (Fig 1A–F), consistent with the mRNA patterns reported previously (Brose et al., 1999). To show the specificity of the β-galactosidase antibody labeling, we also labeled with Islet-1 antibody on wild-type spinal cord sections. There was no β-galactosidase expression on Islet-1$^+$ spinal motor neurons and axons of wild-type embryos (Suppl. Fig. 1).

In addition, as we reported in a previous study (Lee et al., 2015), immunostaining on spinal cord sections (Fig 1G, H) and dissociated spinal motor neurons (Fig 1I, J) with anti-Robo1

and anti-Robo2 antibodies showed that both Robo1 and Robo2 receptors were localized on the cell membrane of motor neuron cell bodies and axons. We observed the same Robo1 and Robo2 expression pattern in all spinal cord regions including cervical, brachial, thoracic, and lumbar levels (data not shown). We verified that Robo1 and Robo2 were not expressed by Islet1^{+} spinal motor neurons of Robo1/2 double mutant embryos (Suppl. Fig. 2). We also confirmed that Islet-1^{+} spinal motor neurons were located just outside the Slit1-expressing floor plate (Fig 1K–M). On the other hand, Slit2 was expressed by spinal motor nuclei and the medial floor plate (Fig 1N).

Together, the expression pattern of Robo1 and Robo2 receptors on spinal motor neurons implies that these cells are potentially responsive to repulsive Slit signals.

Motor exit points shift ventrally in Robo or Slit mutants

Since both Robo1 and Robo2 were expressed by spinal motor neuron cell bodies and their axons, we tested whether Robos were involved in regulating the position of motor exit point using Robo1/2 double mutant embryos. As motor axons exit from the spinal cord and project toward their targets at an early embryonic stage, E10.5 embryos were collected and analyzed. The brachial level of the spinal cord was used to compare a consistent level of the spinal cord. In wild type embryos, exit points were quite narrow, with very low variations in position, suggesting that precise mechanisms set the position of exit points. βIII-tubulin labeling on spinal cord sections showed that motor exit points shifted ventrally in *Robo1*$^{-/-}$;*2*$^{-/-}$, closer to the floor plate (Fig 2B). The distance from the ventral midline to the most ventral exit point was significantly decreased in *Robo1*$^{-/-}$;*2*$^{-/-}$ compared to littermate controls (Fig 2F, d_{nv}, *Robo1*$^{+/-}$;*2*$^{+/-}$ = 0.355 + 0.007, n=8 embryos, vs *Robo1*$^{-/-}$;*2*$^{-/-}$= 0.26 + 0.011, n=10 embryos, $P < 0.001$). There was no significant difference between *Robo1*$^{+/-}$;*2*$^{+/-}$ and *Robo1*$^{+/+}$;*2*$^{+/+}$ (0.36 + 0.008, n=8 embryos), suggesting that one copy of each Robo1 and Robo2 are sufficient to guide motor axons to their normal exit position. In addition, the distance from the midline to the average position of all of the exiting motor axon bundles was also significantly decreased in *Robo1*$^{-/-}$;*2*$^{-/-}$ compared to littermate controls (Fig 2G, d_{na}, *Robo1*$^{+/-}$;*2*$^{+/-}$ = 0.385 + 0.007, n=8 embryos, vs *Robo1*$^{-/-}$;*2*$^{-/-}$= 0.317 + 0.006, n=10 embryos, $P < 0.001$).

We also tested whether Slit mutant embryos have the same ventral deviation. We found that exit points shifted ventrally when Slit1 and Slit2 are missing (Fig 2D). The distance from the ventral midline to the most ventral exit point was significantly decreased in *Slit1*$^{-/-}$;*2*$^{-/-}$ compared to littermate controls (Fig 2F, d_{nv}, *Slit1*$^{-/-}$;*2*$^{+/-}$ = 0.373 + 0.007, n=6 embryos, vs *Slit1*$^{-/-}$;*2*$^{-/-}$= 0.299 + 0.006, n=10 embryos, $P < 0.01$). There was no significant difference between *Slit1*$^{-/-}$;*2*$^{+/-}$ and *Slit1*$^{-/-}$;*2*$^{+/+}$ (0.366 + 0.006, n=6 embryos) and the distance was not different from wild-type embryos (Fig 2F). Also, the average distance from the midline to the average position of all of the exiting motor axon bundles was significantly decreased in *Slit1*$^{-/-}$;*2*$^{-/-}$ compared to littermate controls (Fig 2G, d_{na}, *Slit1*$^{-/-}$;*2*$^{+/-}$ = 0.393 + 0.007, n=6 embryos, vs *Slit1*$^{-/-}$;*2*$^{-/-}$= 0.349 + 0.006, n=10 embryos, $P < 0.01$). Interestingly, the distance from the midline to the most ventral exit was significantly decreased in *Slit1*$^{+/+}$;*2*$^{-/-}$ compared to littermate controls (d_{nv}, *Slit1*$^{+/+}$;*2*$^{+/-}$ = 0.365 + 0.008, n=8 embryos, vs *Slit1*$^{+/+}$;*2*$^{-/-}$ = 0.31 + 0.007, n=8 embryos, $P < 0.01$). Together, these results suggest that one copy of

Slit2 is sufficient to guide motor axons to exit at a proper position and Slit1 is not necessary for regulating motor exit points. We also normalized by the width of spinal cord by using both dorsal horn (narrow width) and ventral horn (wide width) and carefully compared to the distances normalized by the spinal cord height. This alternative normalization procedure resulted in the same statistical significance, in that the levels of decrement (ventral-shift) in Slit1−/−;2−/− or Robo1−/−;2−/− were not significantly different when we normalized by the width of spinal cord (data not shown).

The βIII-tubulin labeling clearly showed shifts in spinal motor exit points in Robo1/2 double mutants. However, to observe the trajectories of motor axons toward their exit points more specifically, we used the motor neuron-specific transgenic reporter Isl1^{MN}-GFP (Lewcock et al., 2007) in a Robo1/2 mutant background. In Robo1/2 mutants at the earliest stage of exiting, E9.5 in the spinal cord, the Isl1-GFP^{+} marker clearly showed that motor neurons projected axons that shifted ventrally and exited over a wider area (Fig. 3B). Using Image J, we measured angles of axon bundles projecting within E10 spinal cords. In wild type embryos, the internal axon projection angles were nearly horizontal, and had low variability compared to the mean angle (Fig. 3C, G, and I, n=8 embryos, −17.52 + 2.7°). In mutant embryos, however, the angles were diagonal and more widely varying from the mean angle (Fig. 3D, H, and I, n=8 embryos, −49.55 + 6.1°), suggesting that axon projections were misguided in the absence of Robo receptors. In addition, we measured the thickness of exit points, from the most ventral to the most dorsal exiting bundles. In Robo1/2 double mutants, the thickness was significantly increased compared to wild type embryos (Fig. 3C, D, and J, n=8 embryos for each genotype, $Robo1^{+/+};2^{+/+}$ = 38.82 + 1.14 μm, vs $Robo1^{-/-};2^{-/-}$= 76.79 + 3.58 μm, $P < 0.001$), showing defasciculated motor projections at exit points in the absence of Robo receptors.

To examine the consequences of abnormal motor exit point and misguided motor axons, we collected Isl1-GFP^{+} spinal cords at E12.5 when motor axons projected to the dermomyotome (DM) and ventrally to the body wall. First, we examined the expression patterns of Slits in the spinal cord at E12.5. Both *in situ* and GFP reporter gene labeling clearly showed expression in the floor plate and motor neurons themselves, but in comparison, that there is little to no expression of Slits outside the spinal cord at this stage (Suppl. Fig. 3). In wild-type, tightly bundled Isl1-GFP^{+} motor axons projected to the DM and body wall (Fig. 4A, D). In Robo1/2 double mutants, few motor axons grew toward the DM. This stalling phenotype was observed all of the Robo1/2 double mutants at E12.5 (Fig. 4B, E, n=6 of 6 embryos). In addition, we observed enhanced defasciculation within the choice point, leading to an extensive ventral ramus in the mutants (Fig. 4B). Thickness at exit points was significantly increased in mutants compared to their littermate controls (Fig. 4F, $Robo1^{+/+};2^{+/+}$ = 42.09 + 2.23, vs $Robo1^{-/-};2^{-/-}$ = 72.13 + 5.34, $P < 0.001$). In addition, thickness at choice points was significantly increased in mutants (Fig. 4G, $Robo1^{+/+};2^{+/+}$ = 42.09 + 2.23, vs $Robo1^{-/-};2^{-/-}$ = 72.13 + 5.34, $P < 0.001$). Interestingly, a subset of misguided motor axons entered the DRG, while rarely others exited inappropriately close the floor plate (Fig. 4B, C).

Together, these findings show that repulsive Slit/Robo signals are required to guide ventral motor axons to their precise exit points, and keep motor axons in their proper trajectories in the spinal cord.

Motor exit points shift dorsally in Netrin-1 or DCC mutants

The ventral shifting of motor exit points in the absence of repulsive Slit/Robo signals suggests that the ventral tissue in the spinal cord has an attractive effect on the position of exit points. Since Netrin-1 is one of major attractive guidance cues produced both by the floor plate (Kennedy et al., 2006; Serafini et al., 1996) and by neural progenitors that constitute the ventral and lateral tissues in the neural tube (Dominici et al., 2017; Varadarajan et al., 2017), we tested if attractive Netrin-1/DCC signals are involved in guiding motor exit points to their proper position.

Since DCC is a receptor that mediates attractive Netrin-1 signals (Keino-Masu et al., 1996), we first determined whether DCC was expressed by spinal motor neurons using immunostaining with Islet-1 and DCC antibodies. DCC receptor was present on both Islet-1^{+} spinal motor neuron cell bodies and axons (Fig 5A), suggesting that exit points could be guided by Netrin-1.

To test whether attractive Netrin-1/DCC signals are involved in defining the position of motor exit points, we analyzed Netrin-1 and DCC mutant embryos. When Netrin-1 or DCC was missing, exit points shifted dorsally compared to their littermate controls (Fig. 5C, E). This result was consistent with our previous findings in which spinal motor neuron cell bodies of Netrin-1 or DCC mutant shifted dorsally (Kim et al., 2015). The distance from the midline to the most ventral exit point was significantly increased in *Netrin-1*$^{-/-}$ (Fig 5G, d_{nv}, *Netrin-1*$^{-/-}$ = 0.425 + 0.007, n=10 embryos, vs *Netrin-1*$^{+/-}$= 0.352 + 0.009, n=8 embryos, P < 0.001) and *DCC*$^{-/-}$ (d_{nv}, *DCC*$^{-/-}$ = 0.422 + 0.008, n=8 embryos, vs *DCC*$^{+/-}$ = 0.355 + 0.01, n=8 embryos, P < 0.01). In addition, there were no significant differences between *Netrin-1*$^{+/-}$ and *Netrin-1*$^{+/+}$ or *DCC*$^{+/-}$ and *DCC*$^{+/+}$ (Fig 5G), suggesting that one copy of Netrin-1 or DCC is sufficient to guide motor axons to their normal exit position. Also, the distance from the midline to the average position of all of the exiting motor axon bundles was significantly increased in *Netrin-1*$^{-/-}$ (Fig 5H, d_{na}, *Netrin-1*$^{-/-}$ = 0.474 + 0.009, n=10 embryos, vs *Netrin-1*$^{+/-}$= 0.39 + 0.01, n=8 embryos, P < 0.001) and *DCC*$^{-/-}$ (d_{na}, *DCC*$^{-/-}$ = 0.461 + 0.008, n=8 embryos, vs *DCC*$^{+/-}$ = 0.399 + 0.011, n=8 embryos, P < 0.01). The alternative normalization using the width of spinal cord resulted in the same statistical significance, in that the levels of increment (dorsal-shift) in Netrin-1−/− or DCC−/− were not significantly different when we normalized by the spinal cord height (data not shown).

To observe the initial trajectories of motor axons as they project within the spinal cord toward their exit points, we also used the $Isl1^{MN}$-GFP in a Netrin-1 mutant background. In Netrin-1 mutants, the Isl1-GFP^{+} marker clearly showed that motor neurons projected axons dorsally with dispersed exit points at the earliest stage of exiting, E9.75 in the spinal cord (Fig. 6, n=6 embryos). We used E9.75 as the earliest stage for Netrin-1 embryos, since commissural axons were not forming at E9.5 and thus genotyping for Netrin-1 mutants was not accurate at this stage. We also measured angles of axon bundles projecting within the E10 spinal cords using Image J. In wild type embryos, the angles of internal axon projection

were nearly horizontal with negative angles (Fig. 6C, G, and I, n=6 embryos, −14.73 + 3.5°). In Netrin-1 mutant embryos, however, the axons had more positive angles (Fig. 6D, H, and I, n=6 embryos, 10.07 + 3.65°), showing dorsal shifting inside the spinal cord in the absence of Netrin-1. In addition, we measured the thickness of exit points at the location where motor axons exit the spinal cord. In Netrin-1 mutants, the thickness was significantly increased compared to wild type embryos (Fig. 6C, D, and J, n=6 embryos for each genotype, *Netrin-1*$^{+/+}$= 39.86 + 1.3 μm, vs *Netrin-1*$^{-/-}$= 64.12 + 4.74 μm, $P < 0.001$), showing defasciculated motor projections at exit points in the absence of Netrin-1.

To test the consequence of abnormal motor exit point and defasciculated motor axons, we collected Isl1-GFP^{+} spinal cords at E12.5. β-galactosidase reporter gene labeling showed that, relative to the strong Netrin1 expression in the floor plate, there was no major Netrin-1 expression in the periphery that are comparable to the floor plate levels at this stage (Suppl. Fig. 3). In wild-type, tightly bundled Isl1-GFP^{+} motor axons projected to the DM and body wall (Fig. 7A, B, C). Instead, defasciculated motor axons at exit points were observed in E12.5 Netrin-1 mutants. (Fig, 7D, E). Indeed, the thickness at exit points was significantly increased in the mutants compared to their littermate controls (Fig. 7G, *Netrin-1*$^{+/+}$= 41.73 + 0.68, vs *Netrin-1*$^{-/-}$= 67.51 + 7.41, $P < 0.05$). Also, we observed enhanced defasciculation within the choice point, leading to extensive ventral ramus in the mutants (Fig. 7F). The thickness at choice points was significantly increased in mutants (Fig. 7H, *Netrin-1*$^{+/+}$= 53.21 + 5.36, vs *Netrin-1*$^{-/-}$= 80.45 + 7.9, $P < 0.05$). Interestingly, motor axons projected toward the DM in all of Netrin-1 mutants (n=6 out of 6 embryos) and thus no stalling phenotype was observed in the mutants at E12.5.

The dorsal shift in Netrin-1 or DCC mutants suggests that spinal motor axons are attracted by Netrin-1. To test for direct effects of Netrin-1, we used explant culture assays for spinal motor axons (Fig. 8). For outgrowth assays, E11 Isl1-GFP^{+} spinal motor nuclei were dissected to exclude the floor plate and cultured for 48 hours with or without Netrin-1 (200 ng/ml) (n=4 different day trials, n=12 explants for each treatment). In the absence of Netrin-1 protein, we determined the average axon length (226.8 + 23.2) and axon numbers (40 + 4.2) from the explants. In the presence of Netrin-1 protein, both axon length and numbers were significantly increased (321.2 + 21.2 and 60.8 + 7.9, respectively). To test directional effects of Netrin-1 on spinal motor axons, explants were co-cultured for 48 hours with COS-7 cells transfected with no plasmid (mock) or Netrin-1 expression plasmid (n=5 different day trials, n=15 explants for each treatment). We observed that more axon outgrowth occurred toward the Netrin-1-expressing COS cell aggregates compared to mock conditions, which had no directional influence (Fig. 8F, G). Thus, our explant assays suggest that Netrin-1 has a positive and direct effect on outgrowth and direction of motor axon projections.

Together, these *in vivo* and *in vitro* findings suggest that attractive Netrin-1/DCC signals are required for setting the position of motor exit points, and are necessary to guide normal motor axon trajectories out of the spinal cord.

Motor exit points are positioned by a balance of Slit/Robo repulsive and Netrin-1/DCC attractive signals

The shifts in opposite directions imply that Netrin-1 and Slit signals are opposing in a balance between attraction and repulsion. On one hand, reduced ventral attraction in Netrin-1 or DCC mutants may cause a dorsal shift because the continuing Slit/Robo repulsion away from the floor plate. On the other hand, reduced floor plate repulsion in Slit or Robo mutants may cause a ventral shift because of the continuing Netrin-1/DCC attraction. In a previous study, we showed that longitudinal pioneer axons navigated through the neural tube using a balance of Netrin-1 attraction and Slit repulsion (Kim et al., 2014). To test whether a similar balance was used to determine the position of motor exits, we used combined mutations. A genetic prediction is that the removal of Netrin-1 signal in Robo1/2 mutants will suppress the Robo mutant ventral shifting phenotype. As shown in Figure 9, we generated combined mutants of Netrin-1 with Robo1 and 2. These triple mutants are feasible because the Robo1 and Robo2 genes are tightly linked and so behave as one locus. Therefore, *Netrin-1*$^{+/-}$*;Robo1*$^{+/-}$*;Robo2*$^{+/-}$ mice would behave genetically as a double heterozygous. Every embryo which lacked Netrin-1 antibody labeling, including Netrin-1/Robo1/2 combined mutants, also showed a severe reduction in the number of spinal cord commissural axons that reach the midline. Therefore, our results show that the effects of Netrin-1 and Robo1 and 2 mutations can be assayed independently, and that Robo mutations are unlikely to suppress (or enhance) the severity of the Netrin-1 commissural axon phenotype.

Combining Netrin-1 and Robo mutations caused a lethal genetic interaction, as few mutant embryos were obtained (even at this early E10.5 stage). Contrary to the predicted 1/16 ratio of triple mutants, we obtained one Netrin-1/Robo1/2 triple mutant out of 99 embryos from 11 litters, as we previously reported (Kim et al., 2014). Interestingly, the triple mutant had exit points located at an intermediate position (Fig 10E, G, d_{nv}= 0.27, d_{na}=0.373), with the position similar to controls, including their littermates that were wildtype (Fig, 10G, d_{nv}= 0.356 + 0.013, d_{na}=0.393 + 0.013, n=6 embryos) or triple heterozygotes (Fig. 10B, G, d_{nv}= 0.359 + 0.013, d_{na}= 0.388 + 0.014, n=6 embryos). However, we still observed the dorsal shift of spinal motor neuron cell bodies in the triple mutant. Indeed, the distance from the midline to the lower edge of the motor column and the circumferential distance between the ventral midline and the lower edge of the motor column were increased in the mutant compared to its littermate control (122% and 19.5%, respectively). The levels of increment were similar to the Netrin-1 mutant which we reported in the previous study (Kim et al., 2015). We also noted that the exit points of the triple mutant were wider than in wild type, with defasciculation (Fig. 10E).

Since reduction in Netrin-1 attraction would be predicted to reduce the ventral-ward attraction elicited by homozygous Robo1/2 mutations, we examined Robo1/2 double mutant embryos with reduced Netrin-1 dose, i.e. *Netrin-1*$^{+/-}$*;Robo1*$^{-/-}$*;2*$^{-/-}$ embryos, which we were able to obtain in sufficient numbers. Interestingly, the location of exit points in *Netrin-1*$^{+/-}$*; Robo1*$^{-/-}$*;2*$^{-/-}$ embryos (Fig. 10D, G d_{nv}=0.33 + 0.015, d_{na}=0.369 + 0.018, n=10 embryos) was significantly recovered compared to *Netrin-1*$^{+/+}$*;Robo1*$^{-/-}$*;2*$^{-/-}$ embryos (Fig. 10A, G, d_{nv}= 0.24 + 0.015, d_{na}= 0.321 + 0.016, n=6 embryos, P <0.001). The exit

points were located close to the normal position, suggesting that a reduction in Netrin-1 attraction largely compensated for the complete loss of Slit repulsion in Robo1/2 double mutants. These results are consistent with a mechanism in which the exit points are positioned by a balance of Slit/Robo repulsive and Netrin-1/DCC attractive signals (Fig. 10F, G).

As an alternative strategy to bypass the lethal genetic interaction of Netrin-1/Robo1/2, we also investigated Netrin-1 and single Robo combination mutants; *Netrin-1*$^{-/-}$*;Robo1*$^{-/-}$ or *Netrin-1*$^{-/-}$*;Robo2*$^{-/-}$. While resulting in less lethality, these single combination mutants also provided a test of the individual roles of Robo1 and Robo2 in guiding motor exit in the spinal cord. Interestingly, both *Netrin-1*$^{+/+}$*;Robo1*$^{-/-}$ (Fig. 11A, F, d_{nv}= 0.372 + 0.011, d_{na}= 0.383 + 0.014, n=6 embryos) and *Netrin-1*$^{+/+}$*; Robo2*$^{-/-}$ (Fig. 11C, F, d_{nv}= 0.352 + 0.007, d_{na}= 0.409 + 0.009, n=6 embryos) mutants had a normal exit position rather than having a ventral shift as we observed in *Netrin-1*$^{+/+}$*;Robo1*$^{-/-}$*;2*$^{-/-}$ (Fig. 10A). Motor exit points of both *Netrin-1*$^{-/-}$*;Robo1*$^{-/-}$ (Fig. 11B, F, d_{nv}= 0.424 + 0.009, d_{na}= 0.491 + 0.012, n=8 embryos) and *Netrin-1*$^{-/-}$*;Robo2*$^{-/-}$ (Fig. 11D, F, d_{nv}= 0.431 + 0.017, d_{na}= 0.49 + 0.011, n=6 embryos) shifted dorsally, similar to their littermate *Netrin-1*$^{-/-}$*;Robo1*$^{+/+}$ and *Netrin-1*$^{-/-}$*;Robo2*$^{+/+}$ single mutants, respectively (Fig. 11F). These results are consistent with redundant genetic functions of Robo1 and Robo2, as only Robo1/2 double mutants show the ventral shift.

Discussion

In forming the motor axon pathway from the motor nuclei in the ventral spinal cord to their peripheral targets, the key first step for motor axons is to extend to the boundary of the nervous system, and to exit to the periphery. However, the molecular signals that guide motor axons to and out of their proper exit points remain largely undefined. In the current study, we undertook both *in vivo* and *in vitro* assays to investigate how spinal motor axons navigated toward and out of ventral exit points, with a focus on the guidance functions of the classical guidance cues, the Slits and Netrin-1.

As summarized in Fig. 12, our main findings are that motor axons are guided to their proper exit points in the spinal cord along trajectories determined by a balance of Slit/Robo repulsion and Netrin-1/DCC attraction, and then exit near this balance point.

Slit repellent signals guide initial motor axon trajectories and influence exit points

The floor plate is a major source of secreted and local signals for growing axons (Colamarino and Tessier-Lavigne, 1995b). Several lines of evidence have pointed to the Slits as important floor plate-derived signals involved in guiding motor axons. Indeed, *in vitro* co-culture explant assays with Slit-secreting cells showed that dorsally-projecting cranial (BM/VM) axons were inhibited and repelled by Slit1 and Slit2 (Hammond et al., 2005). Furthermore, *in vivo* studies using Slit or Robo single mutants and ectopic expression of Slit1 showed motor axon pathfinding errors in the hindbrain (Hammond et al., 2005). Recent mouse studies clearly showed that spinal motor axons projected into the floor plate in Robo1/2 double mutants (Bai et al., 2011; Kim et al., 2015). Together, these *in vivo* and *in*

vitro evidence strongly imply that motor axons are capable of responding to Slit/Robo signals.

Using mouse embryos with mutations in specific guidance cues, in the current study we have investigated whether Slit/Robo signals are involved in guiding the position of ventral motor exits in the spinal cord. In the absence of Robo1 and Robo2 receptors, Islet-1^{MN}-GFP spinal cords clearly showed that internal trajectories of motor axons shifted ventrally. Also, motor axons were defasciculated and some motor axons were misguided, suggesting that Slit/Robo signals are also essential for spinal motor axon fasciculation. Axon fasciculation is a mechanism facilitates growing axons to reach their targets. Slit2 is required for motor axon fasciculation during diaphragm muscle innervation, possibly by Robo signaling promoting axon-axon adhesion (Jaworski and Tessier-Lavigne, 2012). Together, these findings suggest that Slit/Robo signals could regulate spinal motor axon fasciculation. However, the mechanism of how Slit/Robo signals promote fasciculation remains to be elucidated.

In addition, we found ventral shifting only in Robo1/2 double mutants but not in single Robo1 or Robo2 mutants. This finding suggests that either Robo1 or Robo2 receptors are sufficient to keep the proper motor exit position in the spinal cord. Indeed, our β-gal and Robo antibody labels support their overlapping function as both receptors are present on motor neuron cell bodies and axons. Interestingly, the ventral shifting phenotype in Slit1/2 double mutant spinal cords was less severe than Robo1/2 double mutants (Fig. 2F, G). This finding suggests that another Robo ligand, potentially Slit3, may also contribute to set the proper motor exit point in the spinal cord.

While it is commonly stated that the Slits are produced by the floor plate, there is lower but potentially significant levels of Slits expressed by neuroepithelial cells lateral to the floor plate, and Slit2 and Slit3 by the motor neurons themselves. The ventral shifts of motor exit points that are demonstrated in Slit and Robo mutants suggest the Slit/Robo effect is predominantly a repulsive influence that steers the motor axons more dorsally. The consistent shifts in these mutants, cannot be straightforwardly interpreted as floor plate repulsion, because of the broader patterns of potential Slit sources. Which Slit source or combination of sources is crucial for motor exit point positioning will require more sophisticated genetic loss of function approaches in future experiments, such as cell-type specific knockouts.

Netrin-1 attraction also guides motor axon trajectories and the position of motor exit points

The role of Netrin-1 in guiding motor axons has remained unclear, because of diverse roles of Netrin-1 in different subtypes of motor axons. Indeed, Netrin-1 repelled cultured trochlear motor axons (Colamarino and Tessier-Lavigne, 1995a; Varela-Echavarría et al., 1997). However, other studies concluded that cultured spinal motor axons from rat and mouse embryos did not respond to Netrin-1, suggesting that Netrin-1 signals are silenced in spinal motor axons (Bai et al., 2011; Varela-Echavarría et al., 1997). Together, these *in vitro* studies suggest that the role of Netrin-1 in guiding motor axons are varied in different subtypes of motor neurons, perhaps depending upon which Netrin receptors are expressed.

In the present study, we observed a clear *in vivo* requirement for Netrin-1 in spinal motor axons, in which motor exit points shifted dorsally in Netrin-1 or DCC mutants, suggesting a ventral-ward attractive role of Netrin-1/DCC signals in spinal motor axons. The dorsal shifting of motor exit points between Netrin-1 and DCC mutants was similar, suggesting that Netrin-1-induced attraction is mediated mainly by the DCC receptor.

The ventral ward effect of Netrin-1 could be from Netrin-1 locally deposited from either local columns of neuroepithelial cells or from transiting commissural axons, or from relatively short range diffusion of Netrin-1 signal from the floor plate. (Dominici et al., 2017; Hand and Kolodkin, 2017; Varadarajan et al., 2017). However, distinguishing the crucial source of Netrin-1 cue was not possible with the global Netrin-1 mutant that we used in the current study. Thus, the source of Netrin-1 vital for motor exit point positioning needs to be distinguished using more sophisticated genetic loss of function approaches in future experiments, such as cell-type specific knockouts.

To test for direct effects of Netrin-1, we used an explant culture assay for spinal motor axons, and found that Netrin-1 had a positive effect on outgrowth and direction of motor axon growth (Fig. 8). These *in vitro* assays strongly supported the *in vivo* results observed in Netrin-1 mutants, and these results together are consistent with ventrally-directed attraction. The inconsistency between our *in vitro* assay and the previous reports in which cultured spinal cord motor axons showed no responses to Netrin-1 (Bai et al., 2011; Varela-Echavarría et al., 1997) could be explained by specific experimental details. While there are numerous potential experimental issues that could lead to the previous negative results, in our case, positive results were obtained using spinal cords at E11 brachial level tissue, and incubation periods of 48 hours. In addition, our cultured tissue included only spinal motor nuclei, which excluded potentially confounding influences from any additional signals produced by the floor plate. These variances could lead to the discrepancy, however, both *in vivo* and *in vitro* results from the current study evidently showed attractive effects of Netrin-1 on spinal motor axons.

Motor exit points are determined by a balance of opposing Slit and Netrin-1 signals

The opposing shifts between Slit/Robo and Netrin-1 mutants suggest that motor axons navigate using a balance point between these repulsive and attractive signals. Additional evidence for an *in vivo* balancing mechanism comes from Netrin-1/Robo1/2 combined mutants, as their motor exit points are nearly restored to their normal position. This evidence for a relatively simple interaction by summing the effects of opposing repellent and attractive signals is inconsistent with the hierarchical model of Slit/Robo silencing of Netrin attraction first proposed for commissural axons (Stein and Tessier-Lavigne, 2001), and later for spinal motor axons (Bai et al., 2011). Consistent with a midline switch in axon responsiveness to midline cues, post-crossing commissural axons do gain responses to a midline-derived repulsive activity (Zou et al., 2000). However, evidence for Netrin silencing came mainly from *in vitro* experiments on individual cultured axons (Stein and Tessier-Lavigne, 2001). Another set of evidence inconsistent with silencing has come from a study of hindbrain commissural axons, which were shown to continue to use Netrin-1 attraction even after crossing the floor plate (Shoja-Taheri et al., 2015).

Several lines of evidence have shown that Netrin and Slit signals can interact in diverse ways in the different nervous systems, including Slits acting through a co-receptor complex to switch on Netrin attraction for thalamocortical axons, and the opposite effect of Netrin attenuation of Slit repulsion (Bielle et al., 2011; Fothergill et al., 2014; Leyva-Díaz et al., 2014; Morales and Kania, 2016). In addition, the parallel independent Netrin and Slit guidance of fly commissural axons has been reported (Garbe and Bashaw, 2007). Using *in vivo* and *in vitro* experiments on pioneer longitudinal axons in the mouse hindbrain, we similarly showed simultaneous Netrin-1/DCC and Slit/Robo guidance, providing another case of neurons responding to a balance between Netrin-1 attraction and Slit repulsion (Kim et al., 2014). These different consequences of Slits and Netrin-1 signals in the various experimental systems might be due to different concentrations of guidance cues, different combinations of receptors, or diverse signaling cascades in different types of axons.

It is also interesting to note that the Netrin-1/Robo1/2 triple mutant had a clear dorsal shift of spinal motor neuron cell bodies as we observed in Netrin-1 mutants (Kim et al., 2015). However, its motor exit points were not shifted dorsally, as we detected in Netrin-1 mutants, but instead they were located at a normal position. These findings suggest potentially separate mechanisms in positioning cell bodies vs. exit points. Different responses of motor neuron cell bodies and axons might be due to subcellular compartmentalization of responses to these or other cues.

Importantly, motor exit points were properly positioned in the absence of both Netrin-1 and Slit signals (Fig. 10E), implicating that another mechanism can act as a backup system if both Slit and Netrin cues are missing. In fact, spinal motor axon navigation is also dependent on other floor plate-derived signals, such as Sema3A and Ephrins (Bai et al., 2011; Poliak et al., 2015), suggesting that the precise motor exit points could be determined by multiple guidance signals. Furthermore, we observed that spinal motor axons still exited out the spinal cord in our Slit/Robo or Netrin-1/DCC mutants. This finding implies the possibility that other cues that specifically promote or are required for CNS exit, such as SDF-1(Lieberam et al., 2005), retain their function even in the absence of Slits and Netrins. Thus, further studies will be needed to clarify the mechanisms of how motor axons integrate multiple signals to find their proper exit points in the spinal cord.

Abnormal exits could lead to peripheral errors: continued guidance by Slit and Netrin-1

In the current study, we report on early embryonic stages when motor neurons start sending axons out into the periphery. Exiting at abnormal positions could put the axons into abnormal peripheral trajectories, or it could be that motor axons recover their proper pathways. Indeed, we tested at E12.5 when motor axons projected to the dermomyotome (DM) and ventrally to the body wall. Specifically, in Robo1/2 double mutants, we observed atypical projections to the DRG and stalling phenotypes (Fig. 4). In addition, both Robo1/2 double mutants and Netrin-1 mutants showed that motor axons had defasciculated trajectories at exit points, which was followed later by defasciculation and guidance errors at major peripheral choice points (Fig. 4, 7). The errors could be due to reduced axon-axon fasciculation, altered fasciculation that leads to errors in pathway choices, or altered responses to extrinsic cues in the peripheral environment. The mutant lines we used in the

current study are global mutations, and so disrupt guidance signals throughout the peripheral pathways. Therefore, it remains unresolved whether the peripheral errors were caused by the mis-positioning of the exit points, or more directly in subsequent guidance choices by peripheral sources of Slit and Netrin guidance cues. According to our observation of expression patterns of Slits and Netrin-1 at this specific stage, it is difficult to see how there is much Slit and Netrin-1 outside to influence the initial exit point or initial stages of navigation. However, because of the limitations in our assays for Slit and Netrin-1 expression in the periphery, it is not possible to rule out the potential influences of low level sources that could be important for guidance. Indeed, a previous study showed that *Slit2* and Robos were present in peripheral motor axons and this could lead to fasciculation in an autocrine/juxtaparacrine manner (Jaworski and Tessier-Lavigne, 2012). Cell type-specific removal of these peripheral sources would help to resolve these points. Additionally, more localized removal might be a useful tool to overcome the perinatal lethality of these mutants and allow tests of whether motor function is disrupted by abnormal exit points or peripheral guidance errors.

Overall, in the present study we reported an important role of ventral signals in the spinal cord in guiding the proper position of motor axon exits. Our findings suggest that the ability of motor axons exit out at specific positions of the spinal cord is due to a balance between Slit/Robo repulsion and Netrin-1/DCC attraction. This positioning mechanism may act as an important developmental fine-tuning, a possible backup positioning system to add another layer of protection from errors in motor axon pathfinding in the neural tube.

Supplementary Material

Refer to Web version on PubMed Central for supplementary material.

Acknowledgments

The *Robo* and *Slit* mutant founder mice were gifts of Marc Tessier-Lavigne (Stanford; Genentech). The *Netrin-1* and *DCC* mutant mice were gifts of Frederic Charron (ICMR, Montreal CA) and Marc Tessier-Lavigne (Stanford; Genentech). The Islet-1^{MN}-GFP-F mice were gifts of Samuel Pfaff (Salk Institute). Netrin-1 antibody was a generous gift from Tim Kennedy (McGill, Montreal CA). The Robo1 and 2 antibodies were a generous gift from Elke Stein (Yale). Several people in the Mastick lab provided help and discussions on this project, including Brielle Bjorke, Farnaz Shoja-Taheri, Hannah Gruner, Katie Weller, and G. Eric Robinson. This project was supported by NIH RO1 NS054740, R21 NS077169, and RO1 EY025205 to GSM. Use of tissue culture and imaging core facilities was supported by P20 RR-016464, P20 GM103440, P20 GM103554, and P20 GM103650.

Abbreviations

DCC	Deleted in Colorectal Cancer
vMN	ventral motor neuron
dMN	dorsal motor neuron
PS1	Presenilin1
DM	dermomyotome
DRG	dorsal root ganglion

BM	branchial motor
VM	visceral motor

References

Bai G, Chivatakarn O, Bonanomi D, Lettieri K, Franco L, Xia C, Stein E, Ma L, Lewcock J, Pfaff S. Presenilin-Dependent Receptor Processing Is Required for Axon Guidance. Cell. 2011; 144:106–118. [PubMed: 21215373]

Bielle F, Marcos-Mondéjar P, Leyva-Díaz E, Lokmane L, Mire E, Mailhes C, Keita M, García N, Tessier-Lavigne M, Garel S, López-Bendito G. Emergent growth cone responses to combinations of Slit1 and Netrin 1 in thalamocortical axon topography. Curr Biol. 2011; 21:1748–1755. [PubMed: 22000108]

Bravo-Ambrosio A, Mastick G, Kaprielian Z. Motor axon exit from the mammalian spinal cord is controlled by the homeodomain protein Nkx2.9 via Robo-Slit signaling. Development. 2012; 139:1435–1446. [PubMed: 22399681]

Brose K, Bland K, Wang K, Arnott D, Henzel W, Goodman C, Tessier-Lavigne M, Kidd T. Slit proteins bind robo receptors and have an evolutionarily conserved role in repulsive axon guidance. Cell. 1999; 96:795–806. [PubMed: 10102268]

Charron F, Stein E, Jeong J, McMahon A, Tessier-Lavigne M. The morphogen Sonic hedgehog is an axonal chemoattractant that collaborates with Netrin-1 in midline axon guidance. Cell. 2003; 113:11–23. [PubMed: 12679031]

Colamarino SA, Tessier-Lavigne M. The axonal chemoattractant netrin-1 is also a chemorepellent for trochlear motor axons. Cell. 1995a; 81:621–629. [PubMed: 7758116]

Colamarino SA, Tessier-Lavigne M. The role of the floor plate in axon guidance. Annu Rev Neurosci. 1995b; 18:497–529. [PubMed: 7605072]

Cowan C, Yokoyama N, Bianchi L, Henkemeyer M, Fritzsch B. EphB2 guides axons at the midline and is necessary for normal vestibular function. Neuron. 2000; 26:417–430. [PubMed: 10839360]

Culotti J, Merz D. DCC and Netrins. Curr Opin Cell Biol. 1998; 10:609. [PubMed: 9818171]

Dominici C, Moreno-Bravo JA, Puiggros SR, Rappeneau Q, Rama N, Vieugue P, Bernet A, Mehlen P, Chédotal A. Floor-plate-derived netrin-1 is dispensable for commissural axon guidance. Nature. 2017; 545:350–354. [PubMed: 28445456]

Farmer WT, Altick AL, Nural HF, Dugan JP, Kidd T, Charron F, Mastick GS. Pioneer longitudinal axons navigate using floor plate and Slit/Robo signals. Development. 2008; 135:3643–3653. [PubMed: 18842816]

Fazeli A, Dickinson S, Hermiston M, Tighe R, Steen R, Small C, Stoeckli E, Keino-Masu K, Masu M, Rayburn H, Simons J, Bronson R, Gordon J, TessierLavigne M, Weinberg R. Phenotype of mice lacking functional Deleted in colorectal cancer (Dcc) gene. Nature. 1997; 386:796–804. [PubMed: 9126737]

Fothergill T, Donahoo AL, Douglass A, Zalucki O, Yuan J, Shu T, Goodhill GJ, Richards LJ. Netrin-DCC signaling regulates corpus callosum formation through attraction of pioneering axons and by modulating Slit2-mediated repulsion. Cereb Cortex. 2014; 24:1138–1151. [PubMed: 23302812]

Garbe DS, Bashaw GJ. Independent functions of Slit-Robo repulsion and Netrin-Frazzled attraction regulate axon crossing at the midline in Drosophila. J Neurosci. 2007; 27:3584–3592. [PubMed: 17392474]

Grieshammer U, Ma L, Plump A, Wang F, Tessier-Lavigne M, Martin G. SLIT2-mediated ROBO2 signaling restricts kidney induction to a single site. Developmental Cell. 2004; 6:709–717. [PubMed: 15130495]

Hammond R, Vivancos V, Naeem A, Chilton J, Mambitisaeva E, Andrews W, Sundaresan V, Guthrie S. Slit-mediated repulsion is a key regulator of motor axon pathfinding in the hindbrain. Development. 2005; 132:4483–4495. [PubMed: 16162649]

Hand RA, Kolodkin AL. Netrin-Mediated Axon Guidance to the CNS Midline Revisited. Neuron. 2017; 94:691–693. [PubMed: 28521119]

Hirsch MR, Glover JC, Dufour HD, Brunet JF, Goridis C. Forced expression of Phox2 homeodomain transcription factors induces a branchio-visceromotor axonal phenotype. Dev Biol. 2007; 303:687–702. [PubMed: 17208219]

Jaworski A, Tessier-Lavigne M. Autocrine/juxtaparacrine regulation of axon fasciculation by Slit-Robo signaling. Nature Neuroscience. 2012; 15:367–369. [PubMed: 22306607]

Kawasaki T, Ito K, Hirata T. Netrin 1 regulates ventral tangential migration of guidepost neurons in the lateral olfactory tract. Development. 2006; 133:845–853. [PubMed: 16439477]

Keino-Masu K, Masu M, Hinck L, Leonardo E, Chan S, Culotti J, TessierLavigne M. Deleted in Colorectal Cancer (DCC) encodes a netrin receptor. Cell. 1996; 87:175–185. [PubMed: 8861902]

Kennedy TE, Wang H, Marshall W, Tessier-Lavigne M. Axon guidance by diffusible chemoattractants: a gradient of netrin protein in the developing spinal cord. J Neurosci. 2006; 26:8866–8874. [PubMed: 16928876]

Kim M, Farmer WT, Bjorke B, McMahon SA, Fabre PJ, Charron F, Mastick GS. Pioneer midbrain longitudinal axons navigate using a balance of Netrin attraction and Slit repulsion. Neural Dev. 2014; 9:17. [PubMed: 25056828]

Kim M, Fontelonga T, Roesener AP, Lee H, Gurung S, Mendonca PR, Mastick GS. Motor neuron cell bodies are actively positioned by Slit/Robo repulsion and Netrin/DCC attraction. Dev Biol. 2015; 399:68–79. [PubMed: 25530182]

Lee H, Kim M, Kim N, Macfarlan T, Pfaff SL, Mastick GS, Song MR. Slit and Semaphorin signaling governed by Islet transcription factors positions motor neuron somata within the neural tube. Exp Neurol. 2015; 269:17–27. [PubMed: 25843547]

Lewcock JW, Genoud N, Lettieri K, Pfaff SL. The ubiquitin ligase phr1 regulates axon outgrowth through modulation of microtubule dynamics. Neuron. 2007; 56:604–620. [PubMed: 18031680]

Leyva-Díaz E, del Toro D, Menal MJ, Cambray S, Susín R, Tessier-Lavigne M, Klein R, Egea J, López-Bendito G. FLRT3 is a Robo1-interacting protein that determines Netrin-1 attraction in developing axons. Curr Biol. 2014; 24:494–508. [PubMed: 24560577]

Lieberam I, Agalliu D, Nagasawa T, Ericson J, Jessell TM. A Cxcl12-CXCR4 chemokine signaling pathway defines the initial trajectory of mammalian motor axons. Neuron. 2005; 47:667–679. [PubMed: 16129397]

Long H, Sabatier C, Ma L, Plump A, Yuan W, Ornitz D, Tamada A, Murakami F, Goodman C, Tessier-Lavigne M. Conserved roles for slit and robo proteins in midline commissural axon guidance. Neuron. 2004; 42:213–223. [PubMed: 15091338]

López-Bendito G, Flames N, Ma L, Fouquet C, Di Meglio T, Chedotal A, Tessier-Lavigne M, Marín O. Robo1 and Robo2 cooperate to control the guidance of major axonal tracts in the mammalian forebrain. J Neurosci. 2007; 27:3395–3407. [PubMed: 17392456]

Mastick GS, Davis NM, Andrew GL, Easter SS. Pax-6 functions in boundary formation and axon guidance in the embryonic mouse forebrain. Development. 1997; 124:1985–1997. [PubMed: 9169845]

Morales D, Kania A. Cooperation and crosstalk in axon guidance cue integration: Additivity, synergy, and fine-tuning in combinatorial signalling. Dev Neurobiol. 2016

Plump A, Erskine L, Sabatier C, Brose K, Epstein C, Goodman C, Mason C, Tessier-Lavigne M. Slit1 and Slit2 cooperate to prevent premature midline crossing of retinal axons in the mouse visual system. Neuron. 2002; 33:219–232. [PubMed: 11804570]

Poliak S, Morales D, Croteau LP, Krawchuk D, Palmesino E, Morton S, Cloutier JF, Charron F, Dalva MB, Ackerman SL, Kao TJ, Kania A. Synergistic integration of Netrin and ephrin axon guidance signals by spinal motor neurons. Elife. 2015:4.

Rothberg JM, Jacobs JR, Goodman CS, Artavanis-Tsakonas S. slit: an extracellular protein necessary for development of midline glia and commissural axon pathways contains both EGF and LRR domains. Genes Dev. 1990; 4:2169–2187. [PubMed: 2176636]

Serafini T, Colamarino S, Leonardo E, Wang H, Beddington R, Skarnes W, TessierLavigne M. Netrin-1 is required for commissural axon guidance in the developing vertebrate nervous system. Cell. 1996; 87:1001–1014. [PubMed: 8978605]

Sharma K, Sheng HZ, Lettieri K, Li H, Karavanov A, Potter S, Westphal H, Pfaff SL. LIM homeodomain factors Lhx3 and Lhx4 assign subtype identities for motor neurons. Cell. 1998; 95:817–828. [PubMed: 9865699]

Shoja-Taheri F, DeMarco A, Mastick GS. Netrin1-DCC-Mediated Attraction Guides Post-Crossing Commissural Axons in the Hindbrain. J Neurosci. 2015; 35:11707–11718. [PubMed: 26290247]

Stein E, Tessier-Lavigne M. Hierarchical organization of guidance receptors: Silencing of netrin attraction by slit through a Robo/DCC receptor complex. Science. 2001; 291:1928–1938. [PubMed: 11239147]

Varadarajan S, Kong J, Phan K, Kao T-J, Panaitof C, Cardin J, Eltzschig H, Kania A, Novitch B, Butler S. Netrin1 Produced by Neural Progenitors, Not Floor Plate Cells. Is Required for Axon Guidance in the Spinal Cord. 2017

Varela-Echavarría A, Tucker A, Püschel AW, Guthrie S. Motor axon subpopulations respond differentially to the chemorepellents netrin-1 and semaphorin D. Neuron. 1997; 18:193–207. [PubMed: 9052791]

Yee K, Simon H, Tessier-Lavigne M, O'Leary D. Extension of long leading processes and neuronal migration in the mammalian brain directed by the chemoattractant netrin-1. Neuron. 1999; 24:607–622. [PubMed: 10595513]

Ypsilanti A, Zagar Y, Chedotal A. Moving away from the midline: new developments for Slit and Robo. Development. 2010; 137:1939–1952. [PubMed: 20501589]

Zou Y, Stoeckli E, Chen H, Tessier-Lavigne M. Squeezing axons out of the gray matter: a role for slit and semaphorin proteins from midline and ventral spinal cord. Cell. 2000; 102:363–375. [PubMed: 10975526]

Highlights

- Motor exit points shift ventrally in Slit and Robo mutants.
- Motor exit points shift dorsally in Netrin-1 and DCC mutants.
- The precise position of motor exit points is set by a balance between Slit/Robo repulsion and Netrin-1/DCC attraction.

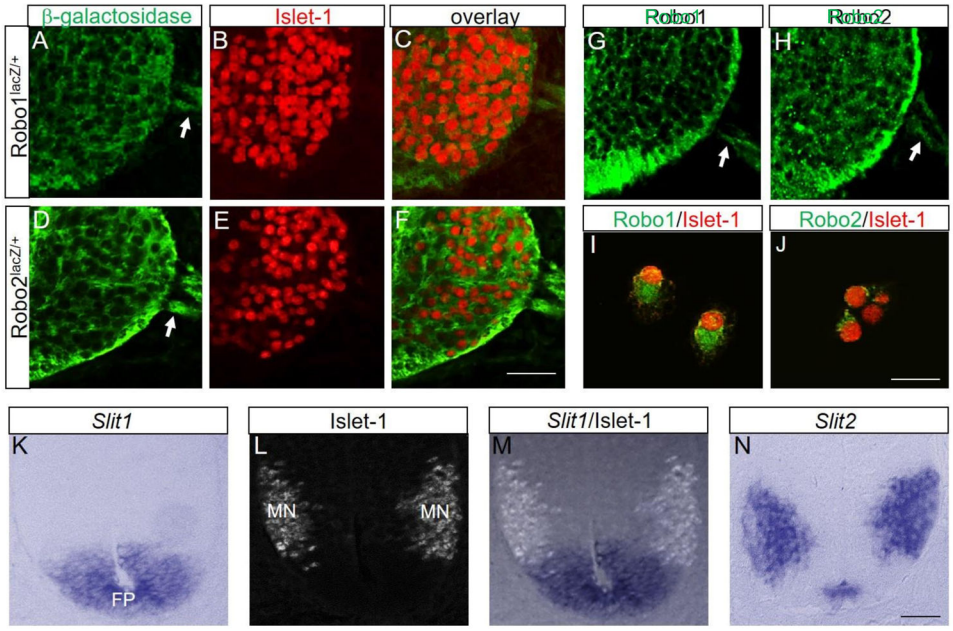

Figure 1. Robos are expressed by spinal motor neurons

(A–F) Islet-1 and β-galactosidase antibody labeling on *Robo1*$^{lacZ/+}$ *and Robo2*$^{lacZ/+}$ E10.5 spinal cord sections (n=4 embryos for each genotype) showing Robos are expressed by spinal motor neurons. (G, H) Robo1 and Robo2 antibody labeling on wild-type E10.5 spinal cord sections. (I, J) Robo1 and Robo2 antibody labeling with Islet-1 on dissociated spinal motor neurons from the wild-type E10.5 spinal cords. (K–M) Islet-1 labeling combined with in situ for *Slit1* mRNA in E10 spinal cord sections. Islet-1^{+} motor neurons settle just outside the Slit1-expressing floor plate. (N) In situ for *Slit2* mRNA in E10 spinal cord sections showing Slit2 is expressed in the medial floor plate and spinal motor neurons. Scale bars: A–H, 50 μm; I, J, 20 μm; K–N, 20 μm. MN, motor neuron; FP, floor plate.

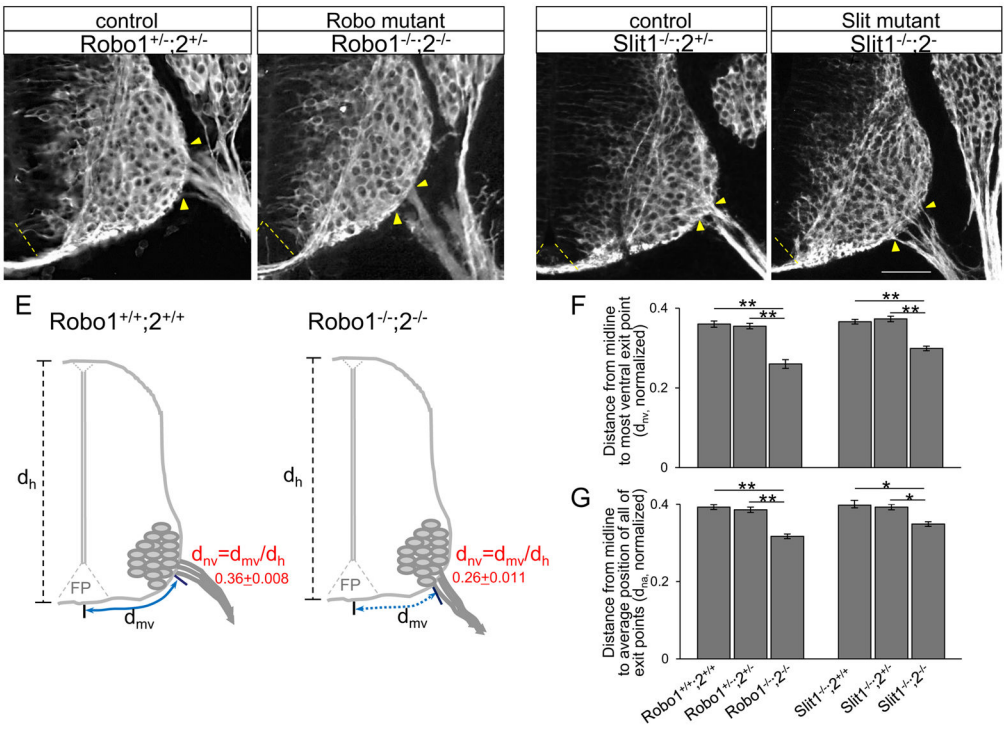

Figure 2. Motor exit points shift ventrally in Robo or Slit mutants

(A–D) βIII-tubulin labeling on spinal cord sections showing motor exit points shift closer to the floor plate in *Robo1*$^{-/-}$;*2*$^{-/-}$ or *Slit1*$^{-/-}$;*2*$^{-/-}$ mutants. *Robo1*$^{+/-}$;*2*$^{+/-}$ (n=8 embryos), *Robo1*$^{-/-}$;*2*$^{-/-}$ (n=10 embryos), *Slit1*$^{-/-}$;*2*$^{+/-}$ (n=6 embryos) and *Slit1*$^{-/-}$;*2*$^{-/-}$ (n=10 embryos). (E) Schematics showing how the measurements are examined in control and *Robo1*$^{-/-}$;*2*$^{-/-}$. The distance from the midline to the most ventral exit point (dmv, solid and dotted blue lines) is normalized by the height (dh)of each embryo (dnv = dmv/dh). (F, G) Summary graphs show the distance from the midline to the most ventral exit point (F), and the distance from the midline to the average position of all of the exiting motor axon bundles (G) in *Robo1*$^{-/-}$;*2*$^{-/-}$ or *Slit1*$^{-/-}$;*2*$^{-/-}$ mutants compared to their littermate controls. Both distances are significantly decreased in Robo or Slit mutants compared to their littermate controls. Yellow arrow heads in A–D show the closest and farthest exit points from the ventral midline. Dotted yellow lines in A–D show the floor plate. Scale bars: A–D, 50 μm. *= $P < 0.01$, ** = $P < 0.001$.

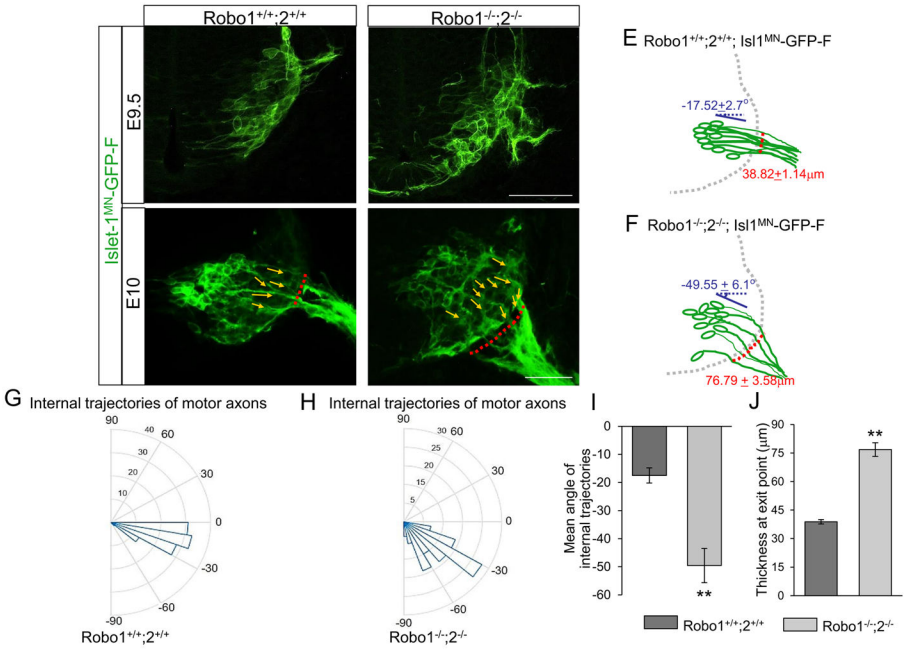

Figure 3. Internal projections of spinal motor axons are abnormal in Robo1/2 double mutants

(A–D) Spinal cord sections of *Robo1*$^{+/+}$;*2*$^{+/+}$*::Islet-1*^{MN}*-GFP-F* and *Robo1*$^{-/-}$;*2*$^{-/-}$*::Islet-1*^{MN}*-GFP-F* embryos (n=8 embryos for each genotype of E9.5 and E10) show that motor axons exit ventrally with wide exit points in *Robo1*$^{-/-}$;*2*$^{-/-}$*::Islet-1*^{MN}*-GFP-F* embryos. Yellow arrows in C and D show individual motor axon trajectories inside the spinal cord. Red dotted lines in C and D show the thickness of exit points (distance between the most ventral and dorsal motor axon bundles). White arrows in B and D show that a subset of motor axons project into the floor plate of *Robo1*$^{-/-}$;*2*$^{-/-}$*::Islet-1*^{MN}*-GFP-F* embryos. (E, F) Schematics of spinal motor axon trajectories (green) of E10 *Robo1*$^{+/+}$;*2*$^{+/+}$*::Islet-1*^{MN}*-GFP-F* and *Robo1*$^{-/-}$;*2*$^{-/-}$*::Islet-1*^{MN}*-GFP-F* embryos. Mean angles of axon projections and thickness of exit points are indicated with blue and red, respectively. (G, H) Rose histograms showing the distributions of angles inside the spinal cord of E10 *Robo1*$^{+/+}$;*2*$^{+/+}$*::Islet-1*^{MN}*-GFP-F* (G, n=6 embryos) and *Robo1*$^{-/-}$;*2*$^{-/-}$*::Islet-1*^{MN}*-GFP-F* (H, n=6 embryos). Angles of each projection are clustered in 10° bins. The length of the radius of each segment represents the percentage of total axons included each bin. Note that the radial lengths are shown on a shorter scale in the mutant graph because the angles were more variable, and therefore had lower percentages per bin. (I) Summary graphs show that mean angles of axon projections shifted ventrally significantly in mutant embryos. (J) Quantification of the thickness of exit points shows that Robo mutants have defasciculated exit points compared to their controls. Scale bars: A, B, 50 μm; C, D: 50 μm. ** = $P < 0.001$.

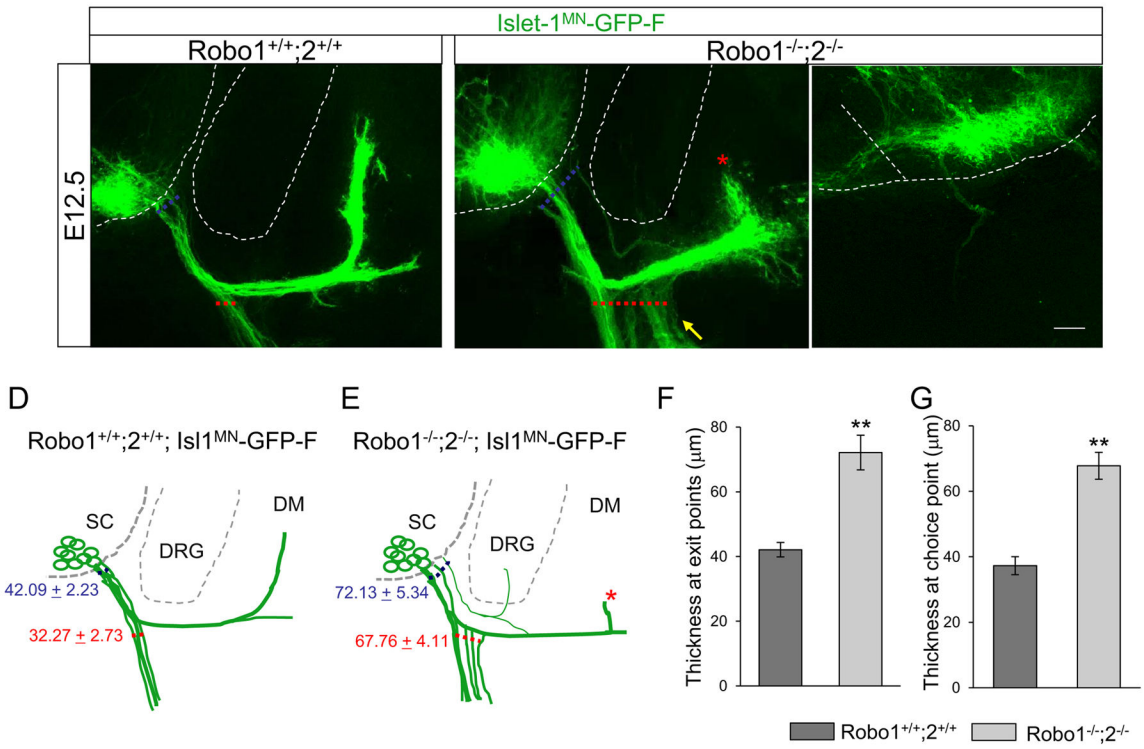

Figure 4. Spinal motor nerve projections are abnormal in Robo1/2 double mutants

(A–C) Spinal cord sections of *Robo1*$^{+/+}$;*2*$^{+/+}$*::Islet-1*^{MN}*-GFP-F* and *Robo1*$^{-/-}$;*2*$^{-/-}$*::Islet-1*^{MN}*-GFP-F* embryos (n=8 E12.5 embryos for each genotype) show that motor trajectories are widely dispersed at the exit points and at the choice points in *Robo1*$^{-/-}$;*2*$^{-/-}$*::Islet-1*^{MN}*-GFP-F* embryos. The white arrow in B shows abnormal projections into the dorsal root ganglion (DRG). The asterisk in B shows that fewer axons grow into the dermomyotome (DM). The yellow arrow in B shows enhanced defasciculation within the choice point, leading to extensive ventral ramus. The white arrow in C shows an example of a motor axon that exits much closer to the FP in *Robo1*$^{-/-}$;*2*$^{-/-}$*::Islet-1*^{MN}*-GFP-F* embryos. (D, E) Schematics of spinal motor axon trajectories (green) in E12.5 *Robo1*$^{+/+}$;*2*$^{+/+}$*::Islet-1*^{MN}*-GFP-F* and *Robo1*$^{-/-}$;*2*$^{-/-}$*::Islet-1*^{MN}*-GFP-F* embryos. The thickness of exit points and choice points are indicated with blue and red, respectively. (F) Quantification of the thickness at exit points (dotted blue lines in A and B) shows that Robo mutants have defasciculated exit points compared to their controls. (L) Quantification of the thickness at choice points (dotted red lines in A and B) shows that defasciculated motor axons project to the body wall in Robo mutants.

Scale bars: A–C, 50 μm. SC, spinal cord; DRG, dorsal root ganglion; DM, dermomyotome; FP, floor plate. ** = $P < 0.001$.

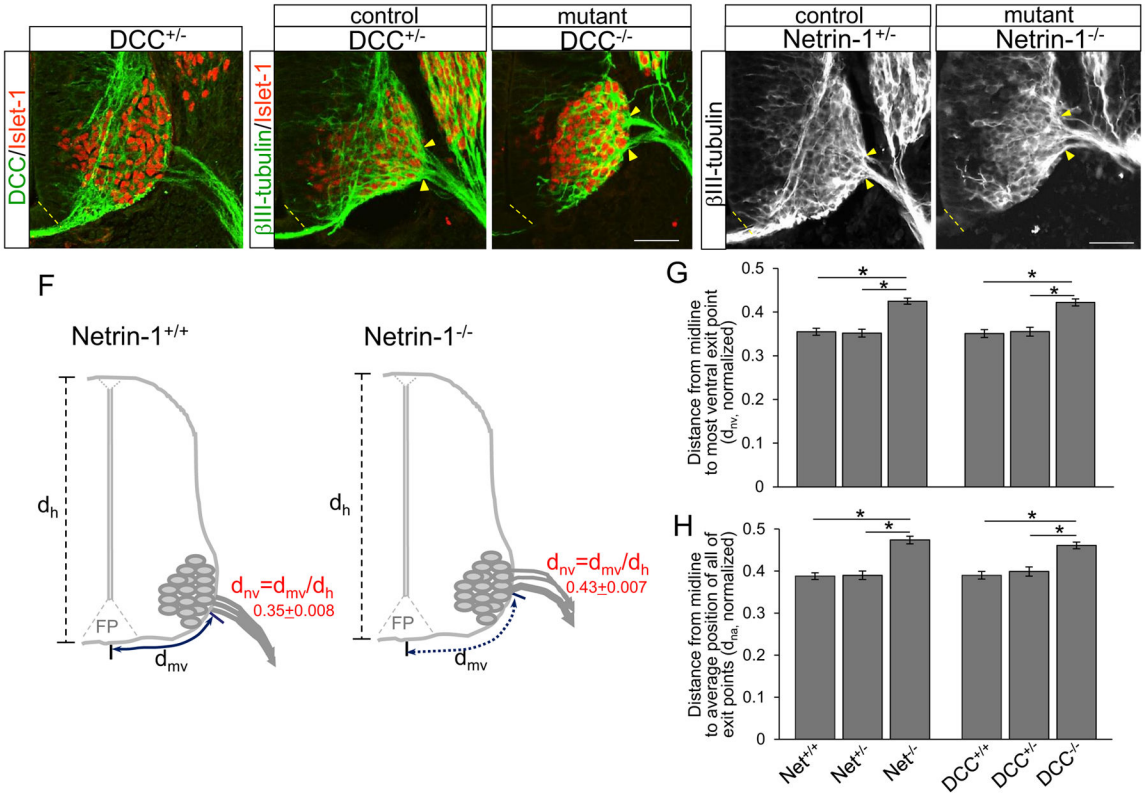

Figure 5. Motor exit points shift dorsally in Netrin-1 or DCC mutants

(A) DCC and Islet-1 labeling of *DCC*$^{+/-}$ E10.5 spinal cord sections showing that DCC is expressed on Islet-1^{+} spinal motor neurons. (B and C) βIII-tubulin and Islet-1 labeling of *DCC*$^{+/-}$ (n=8 embryos) and *DCC*$^{-/-}$ (n=8 embryos) spinal cord sections showing that motor exit points shift dorsally in *DCC*$^{-/-}$. (D and E) βIII-tubulin labeling on *Netrin-1*$^{+/-}$ (n=8 embryos) and *Netrin-1*$^{-/-}$ (n=10 embryos) spinal cord sections showing that motor exit points move away from the floor plate in *Netrin-1*$^{-/-}$ mutants. (F) Schematics showing how the measurements are determined in control and *Netrin-1*$^{-/-}$. The distance from the midline to the most ventral exit point (dmv, solid and dotted blue lines) is normalized by the height (dh) of each embryo (dnv = dmv/dh). (G, H) Summary graphs show the distance from the midline to the most ventral exit point (G), and the distance from the midline to the average position of all of the exiting motor axon bundles (H) in *Netrin-1*$^{-/-}$ or *DCC*$^{-/-}$ mutants compared to their littermate controls. Both distances are significantly increased in *Netrin-1*$^{-/-}$ or *DCC*$^{-/-}$ mutants compared to their littermate controls. Yellow arrow heads in B–E show the closest and farthest exit points from the ventral midline. Scale bars: A–C, 50 μm; D, E, 50 μm. *= $P < 0.01$, ** = $P < 0.001$.

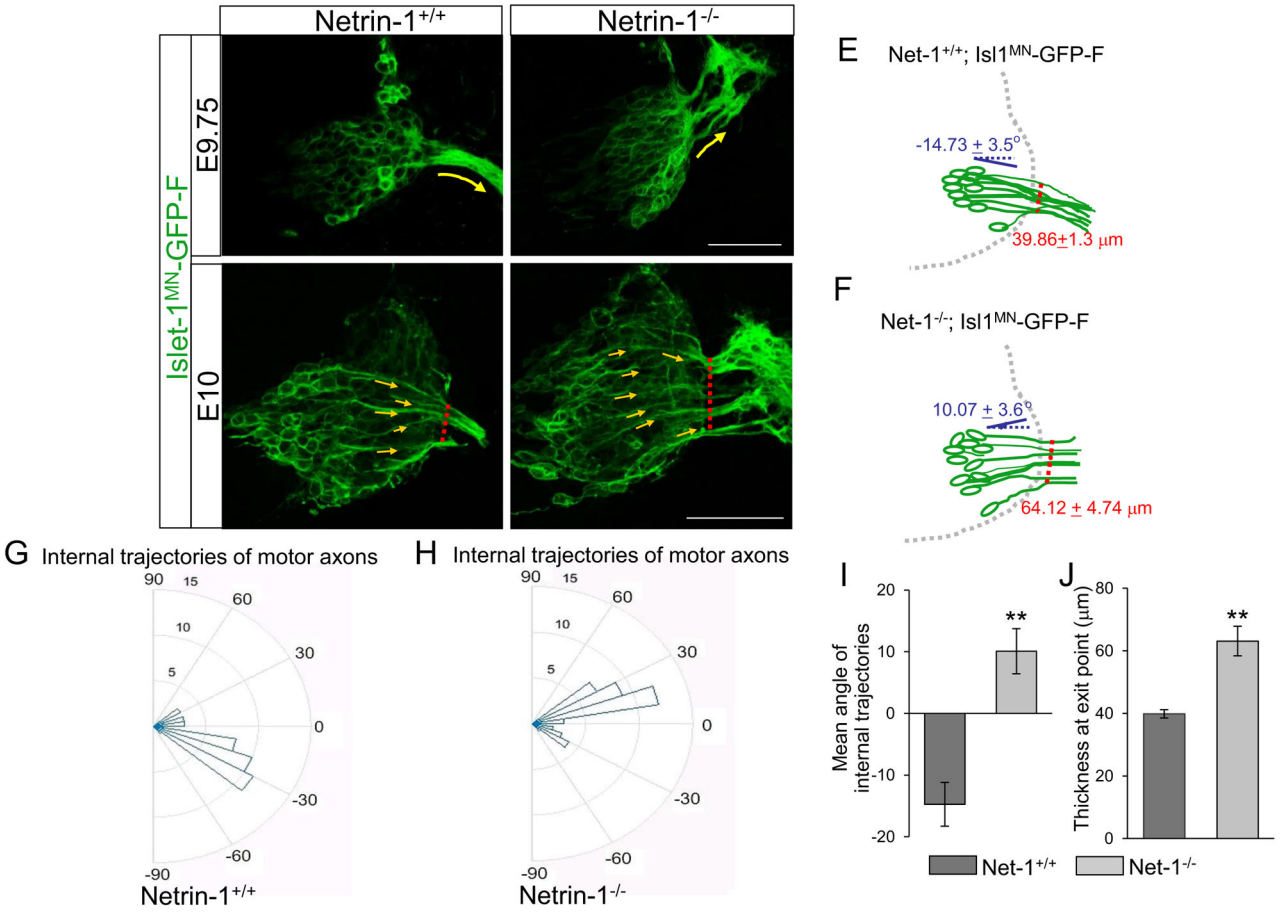

Figure 6. Internal projections of spinal motor axons are abnormal in Netrin-1 mutants

A–D) Spinal cord sections of *Netrin-1*$^{+/+}$*::Islet-1*^{MN}*-GFP-F* and *Netrin-1*$^{-/-}$;*2*$^{-/-}$*::Islet-1*^{MN}*-GFP-F* embryos (n=6 embryos for each genotype of E9.75 and E10; note that these examples appear slightly more advanced than in Fig. 3) show that motor axons exit dorsally with wide exit points in *Netrin-1*$^{-/-}$*::Islet-1*^{MN}*-GFP-F* embryos. Yellow arrows in C and D show individual motor axon trajectories inside the spinal cord. Red dotted lines in C and D show the thickness of exit points. In Netrin-1 mutants, motor axons become disoriented after exit the spinal cord, leading to strong GFP labeling (white arrows in B and D). (E, F) Schematics of spinal motor axon trajectories (green) of E10 *Netrin-1*$^{+/+}$*::Islet-1*^{MN}*-GFP-F* and *Netrin-1*$^{-/-}$*::Islet-1*^{MN}*-GFP-F* embryos. Mean angles of axon projections and thickness of exit points are indicated with blue and red, respectively. (G, H) Rose histograms showing the distributions of angles inside the spinal cord of E10 *Netrin-1*$^{+/+}$*::Islet-1*^{MN}*-GFP-F* (G, n=6 embryos) and *Netrin-1*$^{-/-}$*::Islet-1*^{MN}*-GFP-F* (H, n=6 embryos). Angles of each projection are clustered in 10° bins. The length of the radius of each segment represents the percentage of total axons in each 10° bin. (I) Summary graphs show that mean angles of axon projections significantly increase in mutant embryos. (J) Quantification of the thickness of exit points shows that Netrin-1 mutants have defasciculated exit points compared to their controls. Scale bars: A, B, 50 μm; C, D: 50 μm. ** = $P < 0.001$.

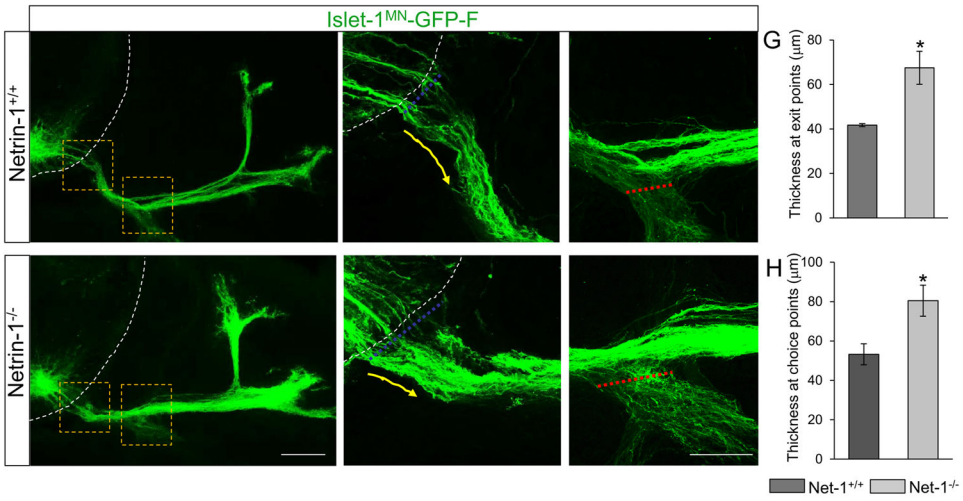

Figure 7. Spinal motor nerve projections are abnormal in Netrin-1 mutants

(A–F) Spinal cord sections of *Netrin-1*$^{+/+}$*::Islet-1*^{MN}*-GFP-F* and *Netrin-1*$^{-/-}$*::Islet-1*^{MN}*-GFP-F* embryos (n=6 embryos for each genotype of E12.5; note that these examples appear slightly less advanced than in Fig 4) show that motor trajectories are widely dispersed at the exit points and at the choice points in *Netrin-1*$^{-/-}$*::Islet-1*^{MN}*-GFP-F* embryos. Dotted white lines in A, B, D, and E show the spinal cord. Yellow arrows in B and E show motor axon trajectories at exit points. (G) Quantification of the thickness at exit points (dotted blue lines in B and E) shows that Netrin-1 mutants have defasciculated exit points compared to their controls. (H) Quantification of the thickness at choice points (dotted red lines in C and F) shows enhanced defasciculation within the choice point, leading to extensive ventral ramus in Netrin-1 mutants. Scale bars: A, D, 100 μm; B, C, E, F, 50 μm. SC, spinal cord; DM, dermomyotome. *=$P < 0.05$.

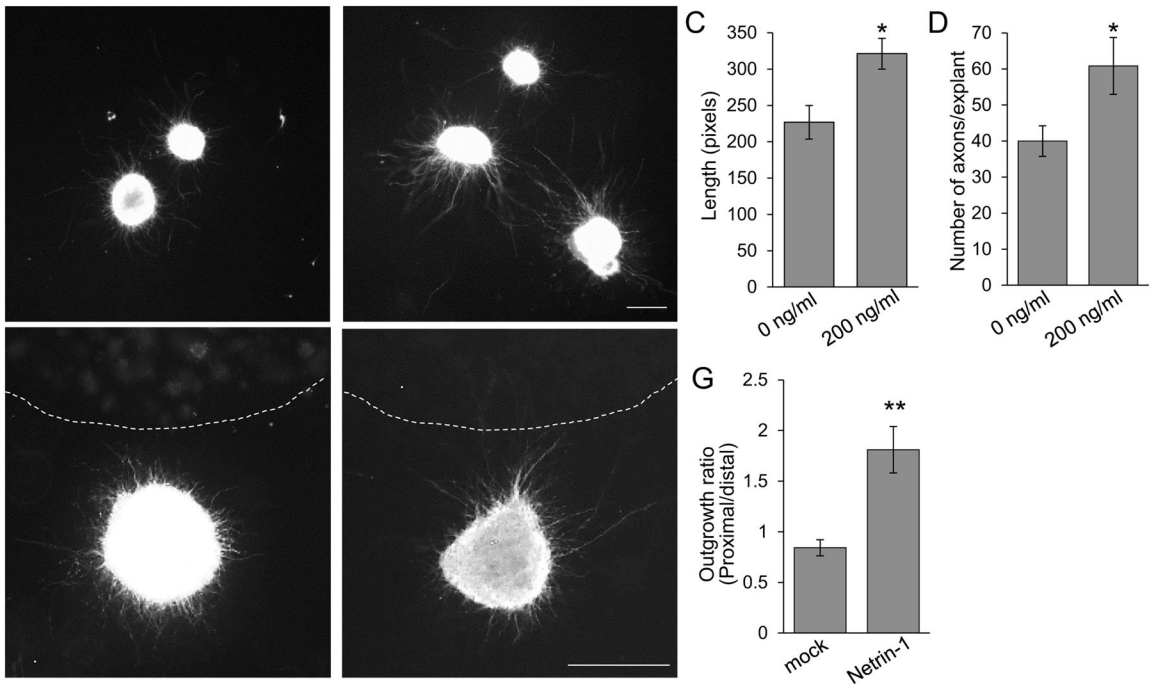

Figure 8. Netrin-1 increases outgrowth of and attracts cultured spinal motor axons

(A, B) Explants of Isl1-GFP^{+} spinal motor nuclei were dissected to exclude the floor plate at E11. Explants were cultured for 48 hrs with or without Netrin-1 (200 ng/ml) (n=4 different day trials, n=12 explants for each treatment). (C) Graph of average axon length of each explant, showing that axons grow about 30% longer in the presence of Netrin-1 protein. (D) Graph of average number of axons in the explant, showing about 30% enhancement of axon numbers when Netrin-1 protein is added in the media. (E, F) Spinal motor nuclei explants were co-cultured with aggregates of COS-7 cells transfected with no plasmid (mock) or Netrin-1 expression plasmid (n=5 different day trials, n=15 explants for each treatment). (G) Quantification of directional axon growth into quadrants toward and away from the COS cells. The outgrowth ratio was calculated by the average axon length in the quadrant toward the COS cells (proximal) divided by the average axon length in the quadrants away from the cue source (distal). In the presence of Netrin-1, the ratio significantly increased, about 2-fold, showing that more axon outgrowth occurred toward the Netrin-1 source. Scale bars: A, B, 50 μm; C, D,50 μm. *=$P < 0.05$; **=$P < 0.001$.

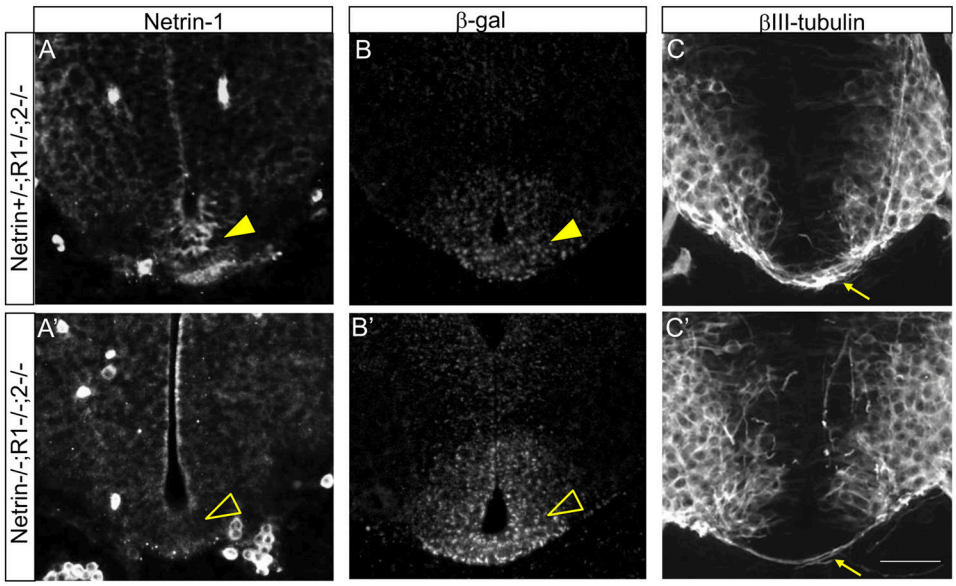

Figure 9. Genotyping of Netrin-1 mutant allele from Netrin-1/Robo combined mutants

(A and A′) Netrin-1 labeling on Netrin-1/Robo1/2 combined mutant spinal cords. In *Netrin-1*$^{+/+}$ or *Netrin-1*$^{+/-}$ spinal cord, the floor plate is Netrin-1 positive (closed arrowhead in A). In *Netrin-1*$^{-/-}$, the floor plate is Netrin-1 negative (open arrowhead in A′). (B and B′) β-gal labeling on Netrin-1/Robo1/2 combine mutant spinal cords. In *Netrin-1*$^{-/-}$ or *Netrin*$^{+/-}$ spinal cord, the floor plate is β-gal positive. However, the intensity of labeling on *Netrin-1*$^{-/-}$ (open arrowhead in B′) is higher than *Netrin-1*$^{+/-}$ (closed arrowhead in B). (C and C′) βIII-tubulin labeling on Netrin-1/Robo1/2 combined mutant spinal cords showing *Netrin-1*$^{-/-}$ spinal cords have none or reduced numbers of commissural axons (arrow in C′) compared to *Netrin-1*$^{+/+}$ or *Netrin-1*$^{+/-}$ (arrow in C). Scale bars: A–C, A′–C′, 50 μm.

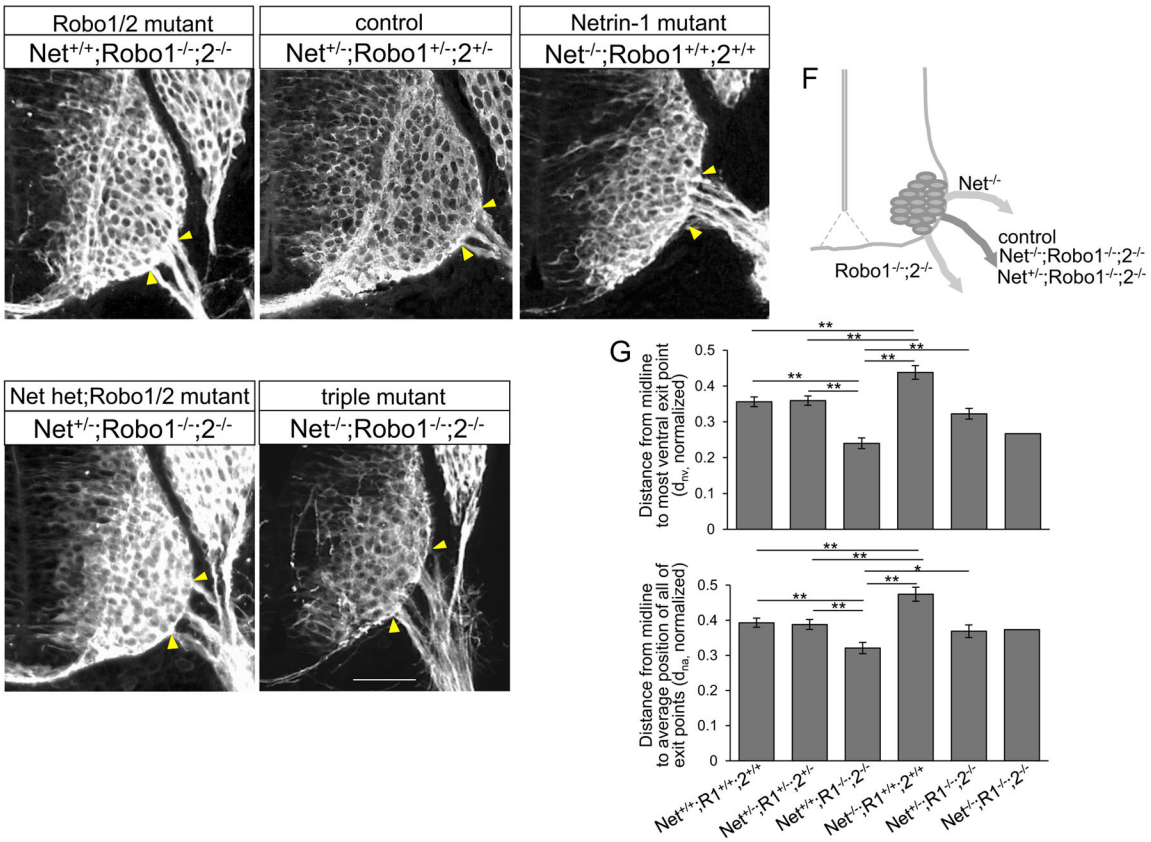

Figure 10. Motor exit points are positioned by a balance of Slit/Robo repulsion and Netrin-1/DCC attraction

(A–E) βIII-tubulin labeling on Netrin-1/Robo1/2 combined mutant spinal cord sections of *Netrin-1*$^{+/+}$*;Robo1*$^{-/-}$*;2*$^{-/-}$ (Robo1/2 double mutant), *Netrin-1*$^{-/-}$*; Robo1*$^{+/+}$*;2*$^{+/+}$ (Netrin-1 mutant), *Netrin-1*$^{+/-}$*;Robo1*$^{-/-}$*;2*$^{-/-}$ (Netrin-1 het; Robo1/2 double mutant) and *Netrin-1*$^{-/-}$*;Robo1*$^{-/-}$*;2*$^{-/-}$ (triple mutant) and their littermate controls, *Netrin-1*$^{+/-}$*;Robo1*$^{+/-}$*;2*$^{+/-}$ showing Netrin-1/Robo1/2 triple mutant has exit points at intermediate positions, similar to its littermate controls. (F) Schematic of locations of motor exit point in control and Netrin-1/Robo1/2 combined mutants. (G) Summary graphs show the distance from the midline to the most ventral exit point, and the distance from the midline to the average position of all of the exiting motor axon bundles in Netrin-1/Robo1/2 combined mutants, *Netrin-1*$^{+/+}$*;Robo1*$^{-/-}$*;2*$^{-/-}$ (n=6 embryos), *Netrin-1*$^{-/-}$*; Robo1*$^{+/+}$*;2*$^{+/+}$ (n=6 embryos), *Netrin-1*$^{-/-}$*;Robo1*$^{-/-}$*;2*$^{-/-}$ (n=1 embryo) and *Netrin-1*$^{+/-}$*;Robo1*$^{-/-}$*;2*$^{-/-}$ (n=10 embryos) compared to their littermate controls, *Netrin-1*$^{+/-}$*;Robo1*$^{+/-}$*;2*$^{+/-}$ and wildtypes (n=6 embryos, respectively). The distances in *Netrin-1*$^{-/-}$*;Robo1*$^{-/-}$*;2*$^{-/-}$ and *Netrin-1*$^{+/-}$*;Robo1*$^{-/-}$*;2*$^{-/-}$ are not significantly different from their littermate controls. Yellow arrow heads show the closest and farthest exit points from the ventral midline. Scale bars: A–E, 50 μm. *= P<0.01, ** = P < 0.001.

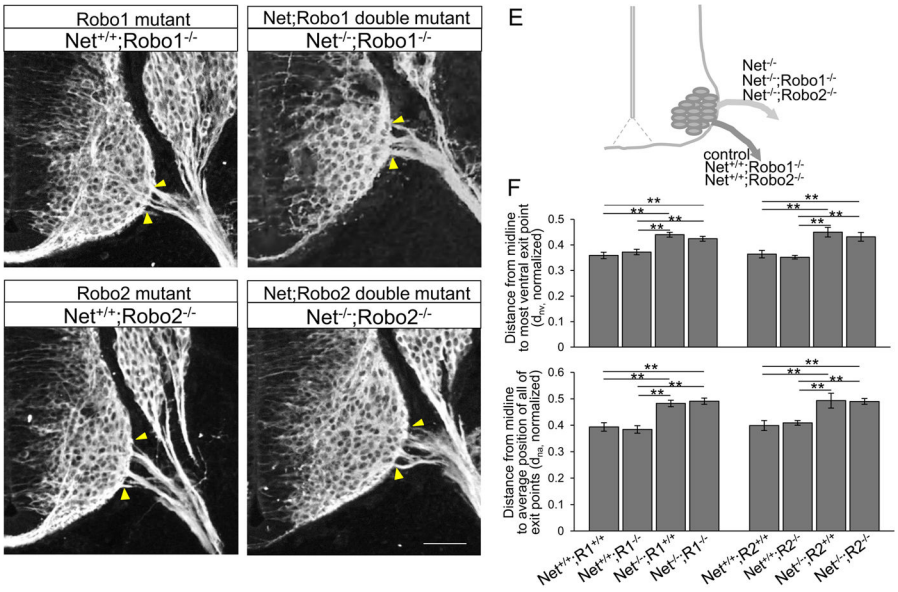

Figure 11. Robo1 and Robo2 receptors have redundant functions to oppose Netrin-1 attraction

(A–D) βIII-tubulin labeling on Netrin-1/Robo1 and Netrin-1/Robo2 combined mutant spinal cord sections shows that motor exit points shift dorsally in *Netrin-1*$^{-/-}$;*Robo1*$^{-/-}$ and *Netrin-1*$^{-/-}$;*Robo2*$^{-/-}$ mutants. (E) Schematic of locations of motor exit point in control and Netrin-1/Robo1 and Netrin-1/Robo2 combined mutants. (G) Summary graphs show the distance from the midline to the most ventral exit point, and the distance from the midline to the average position of all of the exiting motor axon bundles in Netrin-1/Robo1 and Netrin-1/Robo2 combined mutants compared to their littermate controls and Robo1 and Robo2 single mutants, respectively. The distances in *Netrin-1*$^{-/-}$;*Robo1*$^{-/-}$ (n=8 embryos) and Netrin-*1*$^{-/-}$;*Robo2*$^{-/-}$ (n=6 embryos) are significantly increased compared to *Netrin-1*$^{+/+}$;*Robo1*$^{-/-}$ (n=6 embryos) and *Netrin-1*$^{+/+}$;*Robo2*$^{-/-}$ (n=6 embryos), respectively. Yellow arrow heads show the closest and farthest exit points from the ventral midline. Scale bars: A–D, 50 μm. ** = $P < 0.001$.

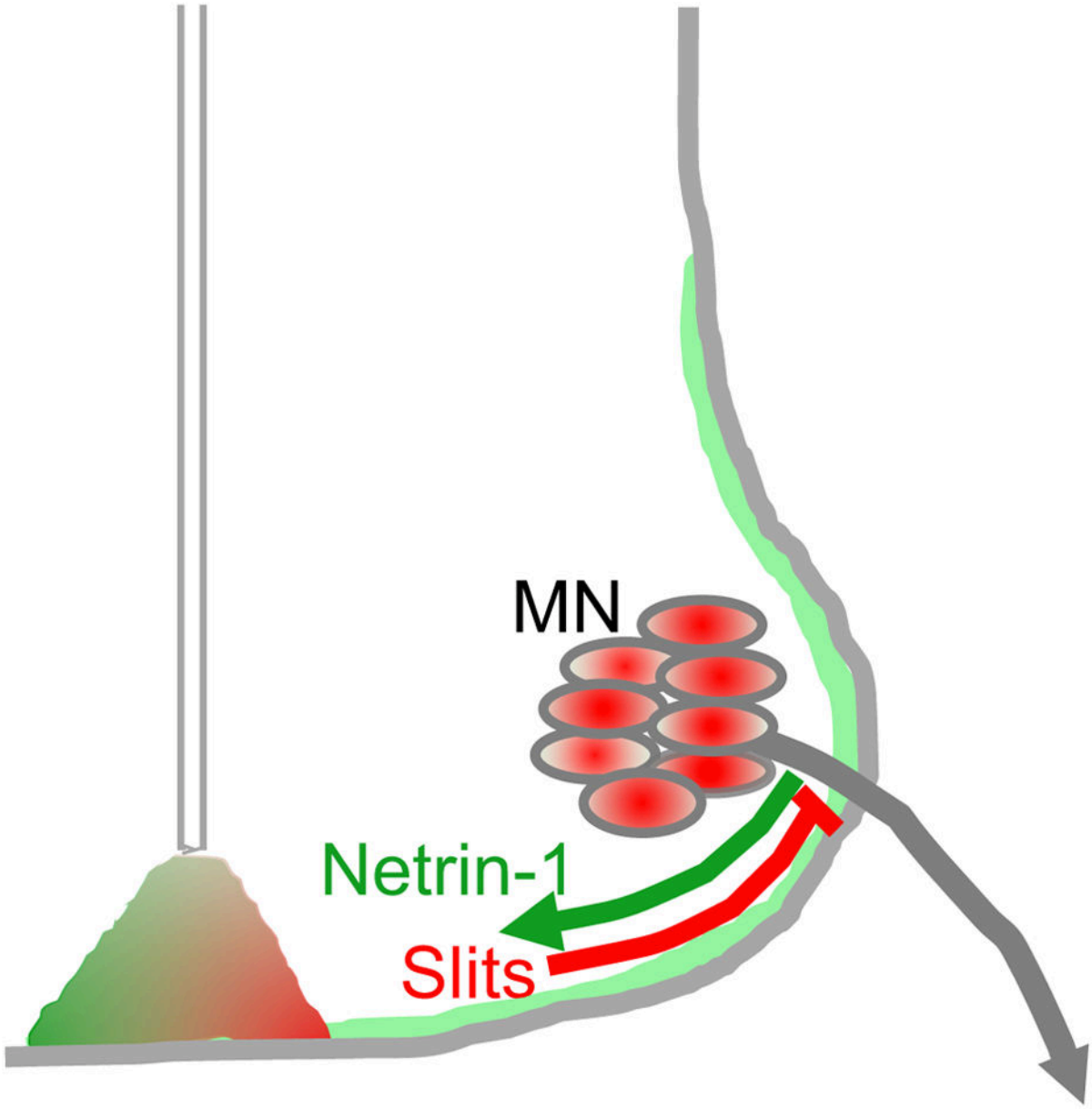

Figure 12. Summary: Opposing Slit/Robo and Netrin-1/DCC guidance signals are required to set the position of motor axon exits in the spinal cord

The position of exit points is determined by a balance of Slit/Robo repulsion (red) and Netrin-1/DCC attraction (green).

Table 1

Genotyping of Netrin-1 mutant allele from Netrin-1/Robo1/2 combined mutants

Genotype	Netrin-1 labeling	β-gal labeling	Commissural axons in the spinal cord
Netrin-$1^{+/+}$	Yes	No	Yes
Netrin-$1^{+/-}$	Yes	Yes	Yes
Netrin-$1^{-/-}$	No	Yes	almost gone